

Monocytes deposit migrasomes to promote embryonic angiogenesis

Received: 24 August 2021

Accepted: 12 October 2022

Published online: 28 November 2022

 Check for updates

Cuifang Zhang¹, Tianqi Li², Shuyao Yin¹, Mingyi Gao¹, Helen He¹, Ying Li¹, Dong Jiang¹, Minghui Shi¹, Jianbin Wang¹ & Li Yu¹ 

Pro-angiogenic factors are key regulators of angiogenesis. Here we report that highly migratory cells patrol the area of capillary formation in chick embryo chorioallantoic membrane. These cells deposit migrasomes on their migration tracks, creating migrosome-enriched areas. Single-cell sequencing identified these cells as monocytes. Depletion of monocytes impairs capillary formation. Quantitative mass spectrometry analysis reveals that monocyte migrasomes are enriched with pro-angiogenic factors. Purified migrasomes promote capillary formation and monocyte recruitment *in vivo*, and endothelial cell tube formation and monocyte chemotaxis *in vitro*. Knockdown or knockout of *TSPAN4* reduces migrasome formation and impairs capillary formation and monocyte recruitment. Mechanistically, monocytes promote angiogenesis via VEGFA and CXCL12 in migrasomes. In summary, monocytes deposit migrasomes enriched in pro-angiogenic factors to promote angiogenesis.

Development of the vascular system is essential for embryonic development¹. Angiogenesis occurs early in development; in fact, the vascular system is the first functional organ that develops in an embryo^{1,2}. Angiogenesis is driven by a set of angiogenic proteins including angiogenic growth factors, chemokines and extracellular matrix proteins^{3–5}. Among them, VEGF plays dominant roles^{6–8}. These factors are often secreted by cells in the vicinity of developing blood vessels, and they then act on receptors on endothelial cells (ECs)^{9,10}. Secreted angiogenic factors, such as isoforms of VEGFs, can bind to the extracellular matrix, thus maintaining a high local concentration and creating a microenvironment for angiogenesis^{11–14}.

The roles of macrophages and monocytes in angiogenesis are well established^{15–17}. For example, in response to various chemoattractants, monocytes extravasate to tumours and mature into tumour-associated macrophages inside tumours, where they promote angiogenesis by secreting various growth factors and cytokines, including VEGFA^{18–20}. Beside angiogenesis during tumorigenesis, macrophages play an important role in peripheral neuron regeneration by promoting vascularization of the bridge region via VEGFA secretion²¹.

Migrasomes are newly discovered organelles of migrating cells. When a cell migrates, numerous long membrane tethers named retraction fibres are pulled out from the trailing edge of the cell. Large vesicles named migrasomes grow on the retraction fibres. Migrasomes are connected to the retraction fibres and contain numerous intraluminal vesicles, which give migrasomes their characteristic morphological feature²². Migrasome formation is dependent on tetraspanins. These proteins form tetraspanin-enriched microdomains, which then assemble into migrasomes^{23,24}. In zebrafish, migrasomes form during gastrulation and then become enriched in a cavity underneath the embryonic shield. Molecules that provide developmental cues, such as the chemokine CXCL12, are highly enriched in these migrasomes. When the migrasomes rupture or leak, they release these ligands, which then act on the surrounding dorsal forerunner cells, thereby affecting organ morphogenesis²⁵. Thus, the migrasome is proposed to be an organelle for cell–cell communication.

In this Article, we found that migrasome formation by monocytes plays an essential role in angiogenesis in chicken embryos. We observed extensive formation of migrasomes by highly migratory cells on the chorioallantoic membrane (CAM) of chicken embryos from day 9.

¹State Key Laboratory of Membrane Biology, Tsinghua University-Peking University Joint Centre for Life Sciences, Beijing Frontier Research Center for Biological Structure, School of Life Sciences, Tsinghua University, Beijing, China. ²School of Life Science, Tsinghua University, Beijing, China.

 e-mail: liyulab@mail.tsinghua.edu.cn

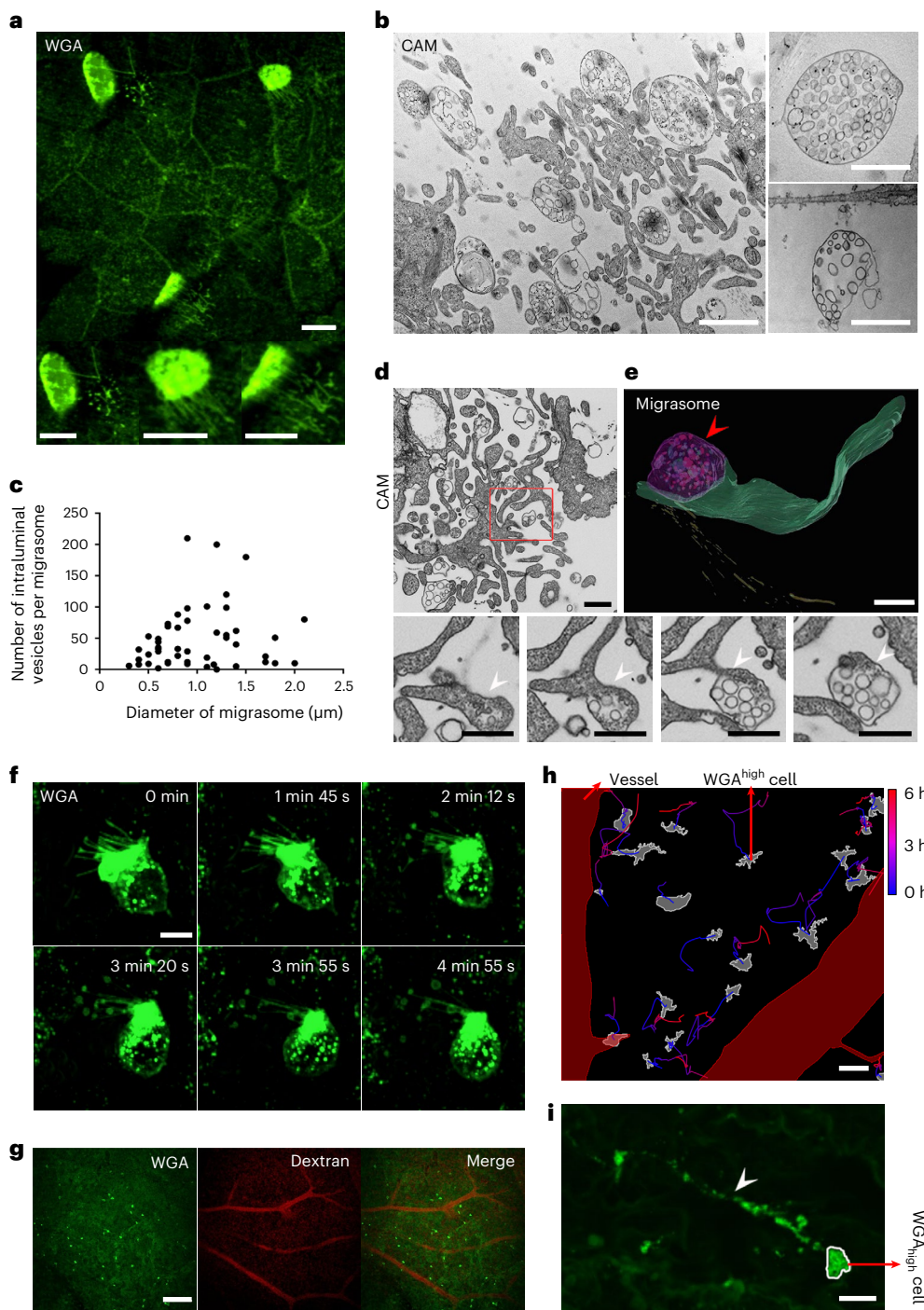


Fig. 1 | Detection of migrasomes in chick embryo CAM. **a**, Confocal image of WGA^{high} and WGA^{low} cells in CAM from a CAM9d. CAM was stained by WGA and observed by spinning disk microscopy. Scale bar, 5 μm . Enlarged images of migrasomes and retraction fibres emanating from WGA^{high} CAM cells are shown at the bottom. Scale bar, 5 μm . **b**, TEM image of CAM9d. Scale bar, 1 μm . Enlarged images of individual migrasomes are shown on the right. Scale bar, 500 nm. **c**, Migrasomes from **b** were quantified for their size and the number of intraluminal vesicles. Sixty migrasomes were examined and quantified. **d**, FIB-SEM analysis of CAM9d. Enlarged z-stack images of the same migrasome (red boxed area) are shown at the bottom to highlight the connection between the migrasome and the retraction fibre. Scale bar, 500 nm. **e**, 3D reconstruction

of a migrasome (red arrowhead). Yellow: collagen fibre; green: retraction fibre. Scale bar, 1 μm . **f**, Migrosome formation captured by spinning disk confocal microscopy. Scale bar, 5 μm . **g**, The distribution of WGA^{high} cells in CAM9d. Blood vessels were revealed by dextran staining. CAM was visualized by Dragonfly confocal z-stack imaging and presented as the maximum intensity projection. Scale bar, 15 μm . **h**, Trajectories of WGA^{high} cells in CAM9d were observed by time-lapse microscopy and analysed by NIS-Elements Viewer. Scale bar, 10 μm . **i**, Enlargement of a WGA^{high} cell in E9d CAM from **h**. The arrowhead indicates a dense patch of migrasomes produced by WGA^{high} cell. Scale bar, 5 μm . Source numerical data are available in source data.

By single-cell sequencing and antibody staining, we identified these highly migratory cells as monocytes. Depletion of monocytes causes impairment of capillary formation, which suggests that these cells

play important roles in angiogenesis. Moreover, we found that migrasomes are capable of inducing angiogenesis *in vivo* and EC tube formation *in vitro*. Knockdown (KD) or knockout of *TSPAN4*, a key gene

for migrasome formation in zebrafish and mammalian cells, blocks migrasome formation and impairs angiogenesis, which can be rescued by adding back purified migrasomes from wild-type CAM. Furthermore, we found that migrasomes can recruit monocytes in vitro and in vivo. KD or knockout of *TSPAN4* significantly reduces the number of monocytes in the area where capillaries are forming. This defect in monocyte recruitment is rescued by adding back migrasomes. The mechanistic basis of these physiological effects is that VEGFA and CXCL12 are enriched in migrasomes. Addition of migrasomes can rescue the phenotypes caused by KD of *VEGFA* or *CXCL12*. Thus, migrasomes carry out their function in recruiting monocytes and promoting angiogenesis through release of CXCL12 and VEGFA, respectively. On the basis of these data, we propose the 'vanguard' model of angiogenesis, in which monocytes prepare a pro-angiogenic microenvironment in advance of angiogenesis by depositing migrasomes enriched in angiogenic factors.

Results

Detection of migrasomes in CAM

Our previous work showed that migrasomes can be detected by staining cells with wheat germ agglutinin (WGA)²⁶. To check whether migrasomes are formed in CAM during embryonic development, we stained CAM from 9-day-old chicken embryos (CAM9d) with WGA ex vivo. WGA staining revealed two types of cells: the majority of cells are large and flat with low WGA signal (WGA^{low}); the other cells are smaller but with a bright WGA signal (WGA^{high}). We found the WGA^{high} cells form retraction fibres and migrasomes (Fig. 1a). To further verify this observation, we carried out transmission electron microscopy (TEM) analysis on CAM9d, which revealed many large vesicles, with diameters up to 2 µm, in the extracellular space (Fig. 1b,c). Consistent with the characteristic morphological features of migrasomes, these vesicles contain numerous intraluminal vesicles, and many of them are adjacent to fibres with diameters of about 50–100 nm (Fig. 1b). To determine the 3D structure of this network of fibres and vesicles, we carried out focused ion beam scanning electron microscope (FIB-SEM) analysis. FIB-SEM showed that these vesicles are connected to fibres and, in many cases, the vesicles are localized on the tips of the fibres (Fig. 1d,e), which is another morphological feature of migrasomes.

To directly observe the formation of migrasomes in vivo, we designed an imaging protocol. First, we cut a hole in the eggshell and stained the CAM with WGA. After staining, we placed the egg on a holder with the hole in direct contact with a cover glass, so that the weight of the egg white and yolk kept the CAM in tight contact with the cover glass. Using time-lapse microscopy, we found that retraction fibres and migrasomes are indeed formed in CAM of living chicken embryos. Put together, these data suggest that migrasomes are formed in CAM by WGA^{high} cells (Fig. 1f and Supplementary Video 1).

We noticed that WGA^{high} cells are evenly distributed in the CAM, and most of them are outside the blood vessels (Fig. 1g). WGA^{high} cells are extraordinarily mobile cells: in some cases, they can move as fast

as 2 µm min⁻¹ (Fig. 1h), and they leave a dense patch of migrasomes in these areas (Fig. 1i).

Migrasomes are generated by monocytes

To investigate the identity of WGA^{high} cells, we first isolated WGA-stained CAM9d from chicken embryos then subjected it to mechanical mincing. The chopped-up CAMs were then treated with collagenase II and trypsin, and the released cells were collected and subjected to fluorescence-activated cell sorting (FACS). The WGA^{high} and WGA^{low} cells were collected and cultured in vitro (Fig. 2a,b). WGA^{high} and WGA^{low} cells have different morphologies (Fig. 2c,d). TEM analysis showed that the migrasomes generated by WGA^{high} cells have a similar morphology to the migrasomes observed in vivo (Fig. 2e). Importantly, WGA^{high} cells generate much higher numbers of migrasomes than WGA^{low} cells (Fig. 2d). Similar to our in vivo observations, cultured WGA^{high} cells move much faster and are smaller than WGA^{low} cells (Fig. 2f and Extended Data Fig. 1a–c). These data suggest that the WGA^{high} cells we isolated are the migrasome-generating WGA^{high} cells we observed in vivo. Next, we subjected the WGA^{high} cells to single-cell RNA sequencing (RNA-seq), which identified two subsets of cells in the WGA^{high} population (Fig. 2g). The first group is enriched with markers for monocytes, while the second group is enriched with markers for epithelium cells (Fig. 2g,h). The RNA-seq results, and the fact that the migrasome-forming WGA^{high} cells are highly migratory, indicate that these cells could be monocytes. To verify the identity of WGA^{high} cells, we carried out immunostaining with KUL01, an anti-macrophage and monocyte monoclonal antibody, and an antibody against CD115, which is expressed by monocytes and macrophages. We found that the WGA^{high} cells did indeed stain positive for both antibodies, which indicates that WGA^{high} cells are monocytes (Fig. 2k). To further verify this, we labelled CAM with anti-CD115 antibody, and sorted out the CD115-positive cells (Fig. 2l). We found that these cells are identical to WGA^{high} cells in terms of morphology and their ability to form migrasomes (Fig. 2j). Finally, we found that WGA^{high} cells are highly phagocytic, and the phagocytosis can be further enhanced by treating WGA^{high} cells with granulocyte–macrophage colony-stimulating factor (GM-CSF) (Fig. 2l,m). Put together, these results indicate that WGA^{high} cells are monocytes.

Monocyte depletion reduces migrasome number

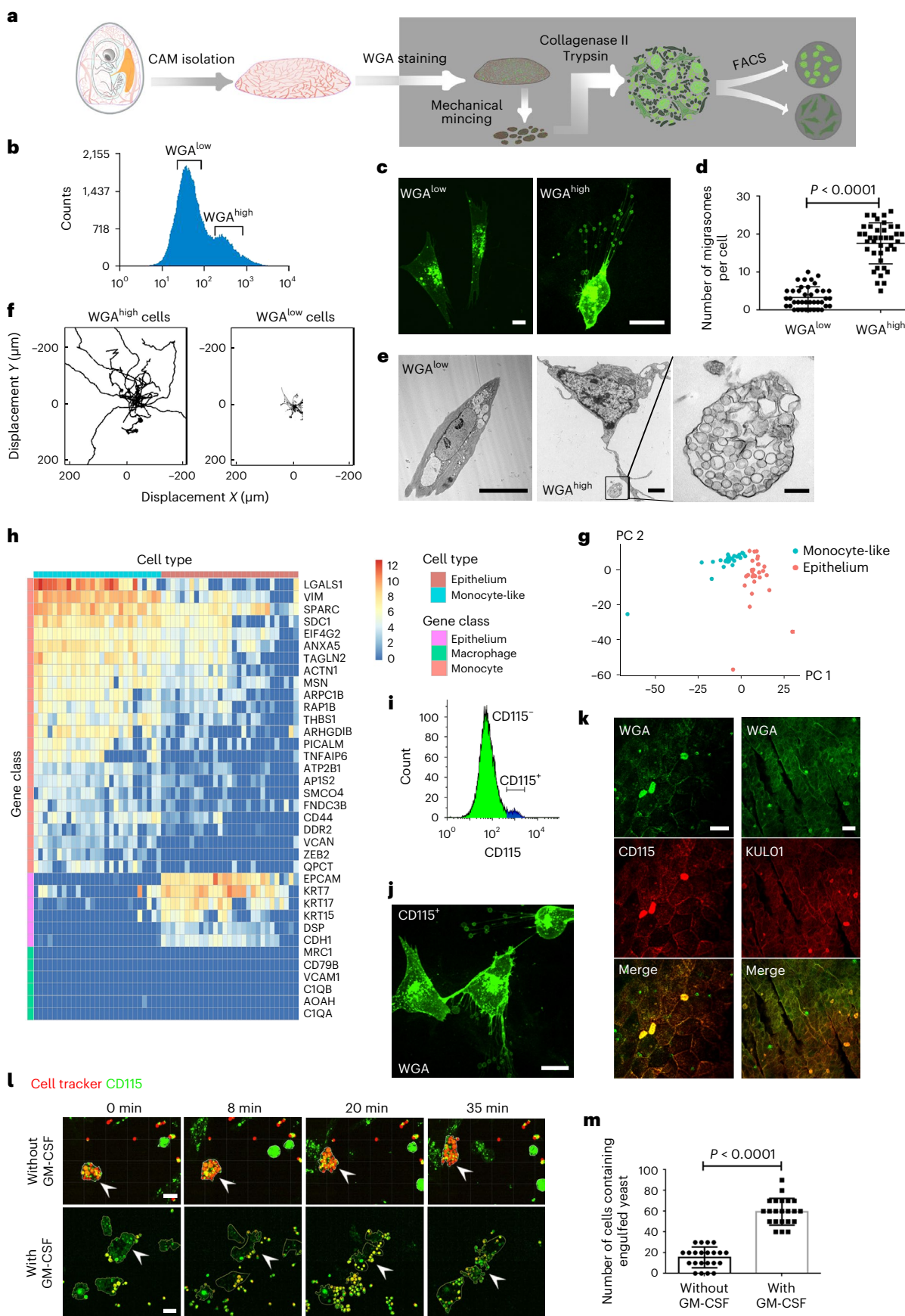
It is well known that a large pool of monocytes is present inside blood vessels. To determine the origin of migrasome-forming monocytes outside blood vessels, we injected the anti-CD115 antibody into blood vessels. Ten minutes after antibody injection, we found that there are indeed large numbers of CD115-positive cells lined up on the wall of blood vessels, and there are no CD115 cells outside blood vessels at this timepoint (Fig. 3a). However, 2 h after injection, many of the CD115-positive cells are found outside the blood vessels, which suggests that the migrasome-forming monocytes in CAM probably come from blood vessels (Fig. 3a). To test the role of monocytes in migrasome formation, we depleted monocytes using liposomes containing the

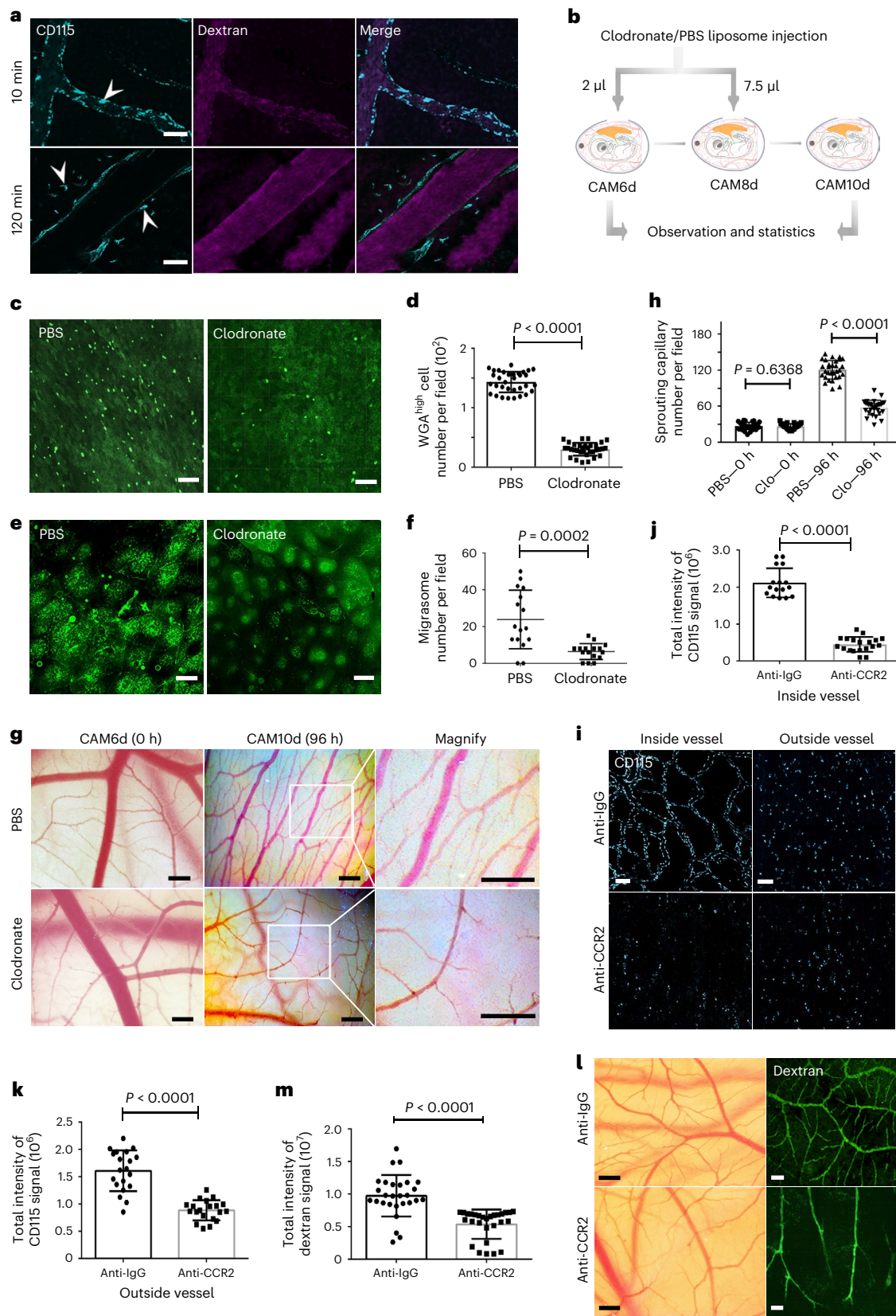
Fig. 2 | Migrasomes are generated by monocytes. **a**, Diagram showing the procedure for isolation of WGA^{high} or WGA^{low} cells from CAM9d. **b**, Isolated cells from WGA-stained CAM9d sorted by FACS according to WGA signal. **c**, WGA^{high} and WGA^{low} cells were observed by confocal microscopy. Scale bars, 10 µm. **d**, Cells from **c** were quantified for the number of migrasomes. Data are presented as mean ± s.e.m.; $n = 40$ cells per group pooled from three independent experiments. $P < 0.0001$, calculated using a two-tailed, unpaired *t*-test. **e**, TEM images of WGA^{high} and WGA^{low} cells. A migrasome from the WGA^{high} cell is shown on the right. Scale bars: 10 µm (left), 1 µm (middle) and 200 nm (right). **f**, Trajectories of cultured WGA^{high} and WGA^{low} cells in the same amount of time (12 h). Twenty cells were examined and quantified in each group. **g**, WGA^{high} cells were subjected to single-cell RNA-seq analysis. Data were analysed by principal component analysis (PCA). **h**, Heat map reporting scaled expression of discriminative marker gene sets for the two cell types identified in **g**. **i**, Cells

isolated from CAM9d were stained by CD115 and sorted by FACS. **j**, The CD115-positive cells were observed by Dragonfly spinning disk confocal microscopy. Scale bar, 5 µm. **k**, CAM9d was stained by WGA and anti-CD115 or KUL01 antibody. Immunofluorescence was visualized in CAMs by confocal z-stack imaging and presented as the maximum intensity projection. Scale bar, 15 µm. **l**, WGA^{high} cells were untreated or treated with GM-CSF for 72 h. Boiled yeast cells (strain BY4741) labelled with a red fluorescent tracer were added. Cells were observed by spinning disk confocal microscopy. White lines indicate the outlines of WGA^{high} cells. White arrows indicate the internalized yeast. Scale bar, 5 µm. **m**, Quantification of the number of monocytes from **l** with engulfed yeast. Data are presented as mean ± s.e.m.; $n = 22$ fields from three independent experiments; P values were calculated using a two-tailed, unpaired *t*-test, $P < 0.0001$. Source numerical data are available in source data.

drug clodronate. The liposomes were microinjected into the CAM blood vessels (Fig. 3b). Five days after the injection, the WGA^{high} cells were almost completely depleted (Fig. 3c,d); moreover, the production

of migrasomes in CAM was significantly reduced (Fig. 3e,f). When we checked angiogenesis, we found that the formation of large blood vessels was not markedly affected by monocyte depletion, but the





formation of capillaries was significantly reduced (Fig. 3g,h). Similar results were obtained using liposomes containing alendronate²⁷, which is less toxic than clodronate (Extended Data Fig. 2a–e). To further verify these findings, we depleted monocytes using an antibody. This is a widely used strategy in immunology, and is considered as a highly specific method to deplete target cells including neutrophils, monocytes

and macrophages^{28,29}. To find an antibody that can deplete monocytes in chicken, we tested all the commercially available antibodies that have been used to label monocytes. As chicken-specific antibodies are very limited, we also included antibodies raised to label monocytes in other species. We found that monocytes in chicken embryos were effectively depleted by an antibody against human CCR2, which was raised using a

Fig. 3 | Depletion of monocytes reduces the migrasome number in CAM and impairs angiogenesis. **a**, Vessels from CAM9d were stained by dextran and CD115. Images were taken 10 or 120 min after staining. Arrowheads indicate the monocytes. Scale bar, 50 μ m. **b**, Diagram of monocytes/macrophages depletion procedure. **c**, The post-treatment CAM10d was stained by WGA488 and visualized by confocal microscopy. Scale bar, 100 μ m. **e**, After monocyte depletion, CAMs were stained by WGA to label migrasomes and imaged by spinning disk microscopy. Scale bar, 10 μ m. **d,f**, The numbers of WGA^{high} cells from **c** or migrasomes from **e** were quantified. Data are presented as mean \pm s.e.m.; $n = 33$ (**d**) or 16 (**f**) fields from three independent experiments; P values were calculated using a two-tailed, unpaired t -test, $P < 0.0001$, $P = 0.0002$. **g**, Post-treated CAMs were visualized with a stereomicroscope. The boxed area is magnified on the right. Scale bar, 500 μ m. **h**, The number of sprouting capillaries from **g** was quantified. Data are presented as mean \pm s.e.m.;

$n = 30$ fields of 30 eggs from three independent experiments; P values were calculated using a two-tailed, unpaired t -test, NS, no significance ($P = 0.6368$), $P < 0.0001$. **i**, Monocyte depletion by anti-CCR2. Vessels from CAM9d were stained inside or outside by CD115-Alexa488 to check the efficiency of monocyte depletion. Scale bar, 50 μ m. **j–k**, The number of monocytes was quantified according to the CD115 signal. Data are presented as mean \pm s.e.m.; $n = 19$ eggs (**j**) and 20 eggs (**k**) from three independent experiments; P values were calculated using a two-tailed, unpaired t -test, $P < 0.0001$. **l**, Post-treated CAMs were visualized with a stereomicroscope (scale bar, 500 μ m) or confocal microscopy after dextran-FITC microinjection (scale bar, 50 μ m). **m**, The number of sprouting capillaries from **l** was quantified according to dextran signal. Data are presented as mean \pm s.e.m.; $n = 28$ fields from 20 eggs from three independent experiments; P values were calculated using a two-tailed, unpaired t -test, $P < 0.0001$. Source numerical data are available in source data.

synthetic peptide corresponding to an *N*-terminal portion of the human CCR2 protein, and has been shown to recognize CCR2 from human and mouse (Fig. 3*i–k*). Similar to the results with clodronate/alendronate liposomes, depletion of monocytes by anti-CCR2 antibody markedly reduced capillary formation (Fig. 3*l–m*). Collectively, these data suggest that monocytes contribute to angiogenesis, which is consistent with previous reports in the literature^{30,31}.

Monocyte migrasomes contain angiogenic factors and chemokine

To study the role of migrasomes in angiogenesis, we isolated migrasomes from CAM9d (Fig. 4*a*). The purity of the isolated migrasomes was analysed by TEM and by western blot for various migrasome markers we reported previously. We found that the isolated migrasomes have the characteristic morphological features of migrasomes (Fig. 4*b*); moreover, migrasome markers are highly enriched in the preparation (Fig. 4*c*)³². Next, we carried out tandem mass tag (TMT) labelling followed by quantitative mass spectrometry (Q-MS; Fig. 4*d*). The resulting volcano plot shows that the protein composition of migrasomes is markedly different from cell bodies (Fig. 4*e*). Known migrasome-enriched proteins such as tetraspanins and integrin β are enriched in CAM migrasomes, while nuclear proteins are depleted (Fig. 4*f*), which suggests that the Q-MS analysis is reliable. Next, we checked whether known angiogenesis factors and chemokines are enriched in migrasomes. Indeed, we found that a host of these factors, including TGF- β 3, VEGFA and CXCL12, are enriched in migrasomes (Fig. 4*f*). It is worth noting that, compared with ECs (the majority of WGA^{low} cells), CXCL12, TGF- β and VEGFA are highly expressed in monocytes (Fig. 4*g* and Extended Data Fig. 3*a*).

Next, we verified the enrichment of these angiogenesis factors and chemokines by western blotting and immunostaining. Owing to the issue of antibody availability, we could test only CXCL12 and VEGFA. We found that both proteins are enriched on migrasomes by western blotting and immunostaining (Fig. 4*h,i*). Next, we stained cryo-sections of CAM with anti-VEGFA and anti-CXCL12 antibodies. We found that monocytes are the main VEGFA- and CXCL12-expressing cells (Fig. 4*j* and Extended Data Fig. 4*a*). We noticed an apparent discrepancy in

the degree of enrichment of VEGFA and CXCL12 signal in western blots and immunostaining. This probably results from an optical illusion created by the method for imaging CAM. The CAM is visualized by z-stack imaging and presented as the maximum intensity projection, which takes the brightest pixel in each layer and displays it in the final 2D image. Thus, thicker objects will look brighter as they have more layers. In this case, the cells are much thicker than migrasomes, and thus appear much brighter when displayed as maximum intensity projection images. It is worth noting that migrasomes from mouse monocytes were also enriched with VEGFA and CXCL12 (Extended Data Fig. 4*b*). This suggests that enrichment of pro-angiogenesis factors in monocyte-derived migrasomes is evolutionarily conserved.

Migrasomes induce capillarization and monocyte recruitment

Next, we tested the role of migrasomes in angiogenesis by adding isolated migrasomes on top of the CAM. To keep the migrasomes in place, we mixed them with Matrigel and added the mixture to the CAM of 9-day-old embryos. As Matrigel can induce angiogenesis by itself, we also delivered the migrasomes by mixing them with low-melting-point agarose. In both cases, adding migrasomes significantly induced capillary formation (Fig. 5*a* and Extended Data Fig. 7*a–d*), which indicates that migrasomes are pro-angiogenic. Furthermore, we found that adding migrasomes significantly enhanced the recruitment of monocyte cells (Fig. 5*j,k*), which suggests that migrasomes act as a chemoattractant for monocytes. In addition to directly observing capillary growth towards migrasomes, which is prone to artefacts, we also carried out the Matrigel invasion assay, in which a nylon mesh coated by a collagen I-Matrigel matrix with or without migrasomes is placed on top of the CAMs, and neovascularization occurs upward and against gravity to invade the matrix. We found that migrasomes significantly promoted capillary formation in this assay (Fig. 5*b,c*).

Migrasomes promote sprouting of ECs ex vivo

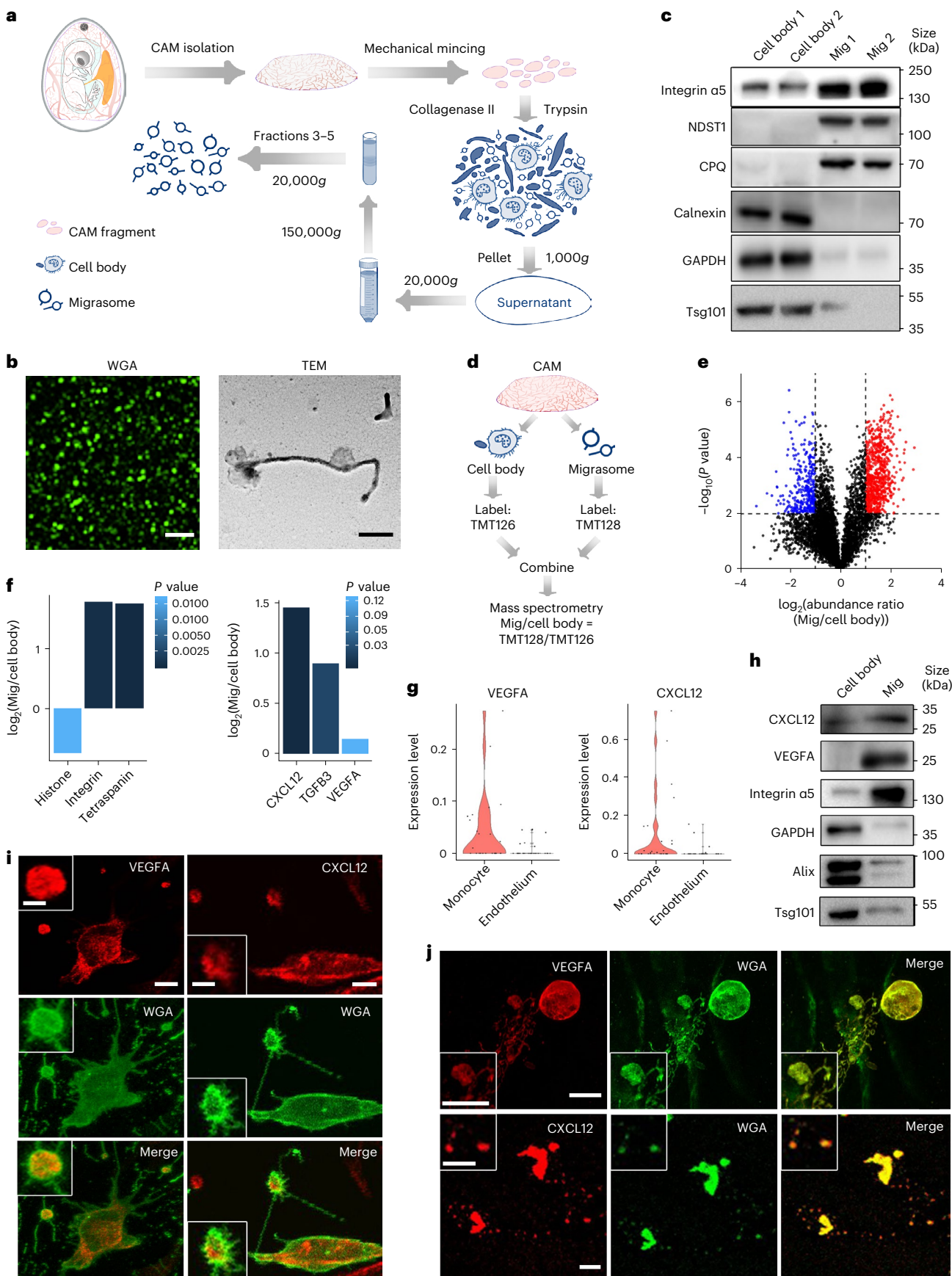
Next, we set up an ex vivo assay that allows us to determine the effect of migrasomes on angiogenesis in more detail. In this assay, CAM from embryonic day 8 (CAM8d) was collected and mounted on top of the

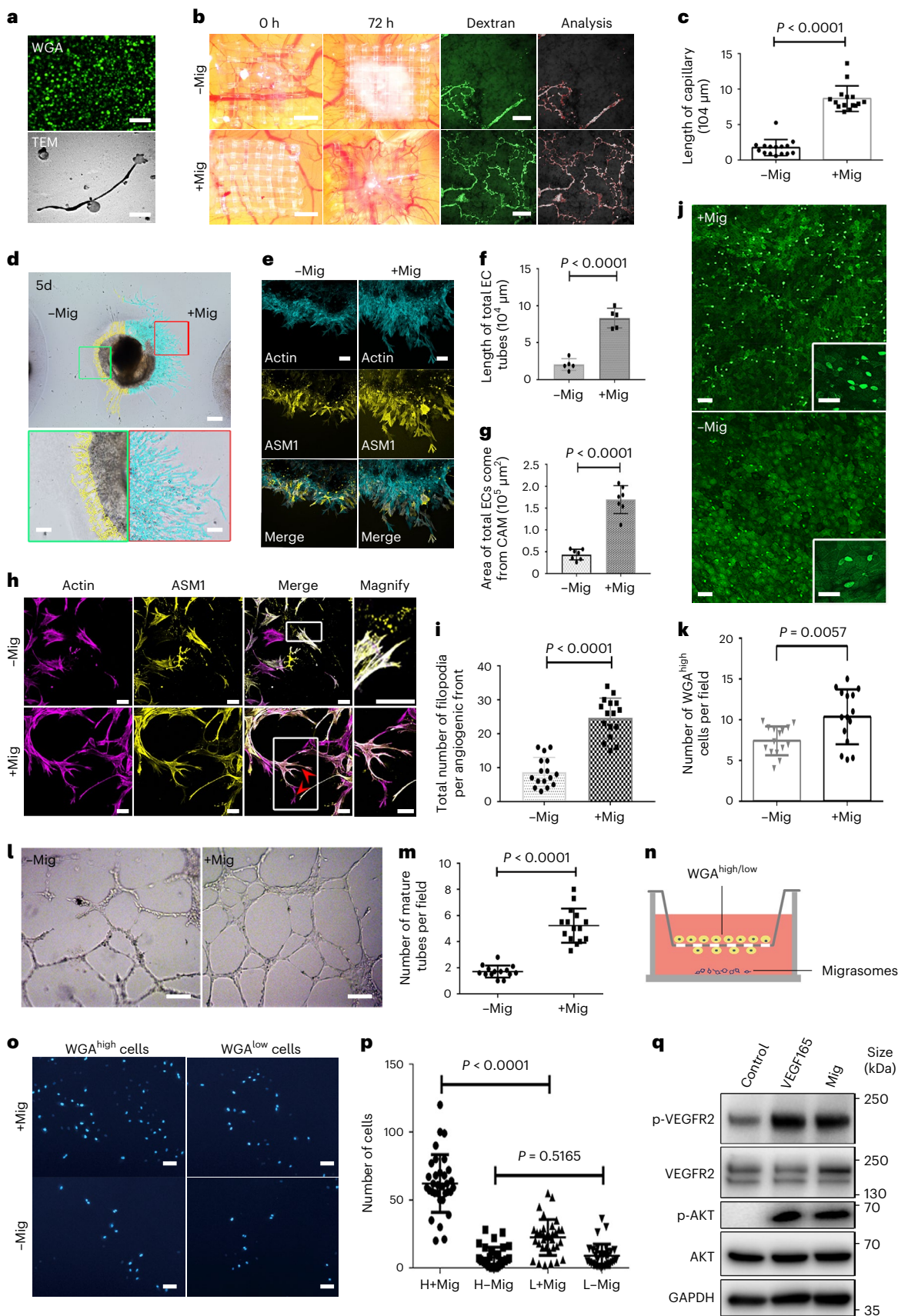
Fig. 4 | Monocyte migrasomes contain angiogenic factors and chemokine. **a**, Diagram of the migrasome (Mig) isolation procedure. **b**, Images of migrasomes purified from CAM9d. Left: confocal image of purified migrasomes stained by WGA; scale bar, 5 μ m. Right: TEM image of migrasomes isolated from CAM9d; scale bar, 500 nm. **c**, Western blot analysis of isolated CAM9d migrasomes with the indicated antibodies. **d**, Diagram of the procedure for TMT labelling and Q-MS. **e**, Volcano plot showing the mass-spectrometry-based quantification of TMT-labelled proteins. The red dots represent a migrasome:cell abundance ≥ 2 , $P < 0.01$; the blue dots represent a migrasome:cell abundance < 0.5 , $P < 0.01$. $n = 6$ biologically independent experiments. P values were calculated in Excel using a two-tailed, two-sample unequal variance t -test. **f**, Data from **e** were analysed for the abundance of the indicated proteins. P values were calculated using a one-tailed, two-sample unequal variance t -test, $P = 0.010823$ (histon);

$P = 0.0000352$ (integrin); $P = 0.00001$ (tetraspanin); $P = 0.000220$ (CXCL12); $P = 0.028115$ (TGF β 3); $P = 0.123519$ (VEGFA). **g**, Violin plots showing the mRNA levels of the indicated genes from single-cell sequencing analysis of monocytes and endothelium cells. **h**, Cell bodies and migrasomes were analysed by western blot using anti-CXCL12 and anti-VEGFA antibodies. **i**, Monocytes isolated from CAM9d were stained with WGA and the indicated antibodies and visualized by confocal microscopy. Scale bar, 5 μ m. Enlarged images of migrasomes are shown in the white boxes. Scale bar, 1 μ m. **j**, CAM9d were stained with WGA and the indicated antibodies. CAM immunofluorescence was visualized by confocal z-stack imaging and presented as the maximum intensity projection. Scale bar, 10 μ m. Enlarged images of migrasomes are shown in the white boxes. Scale bar, 6 μ m. Source numerical data and unprocessed blots are available in source data.

collagen I–Matrigel matrix. Twenty-four hours after mounting, soft agarose with or without migrasomes was placed on opposite sides of the CAM. We reasoned that, if the pro-angiogenesis factors can be released

from migrasomes, they will diffuse from the migrasome-containing agarose and form a gradient in the Matrigel. The diffused factors will attract ECs to migrate out of the CAM towards the source of gradient,





and may also promote proliferation. We found that, 5 days after adding the soft agarose, there were many cells on the side of the CAM close to the migrasome-containing agarose, but not on the side close to the control agarose (Fig. 5d,e). Moreover, cells on the migrasome side

migrated much further from the edge of the CAM compared with cells on the control side (Fig. 5d–g). Time-lapse data showed that, at 2, 4 and 6 days after mounting, the capability of ECs to migrate and possibly proliferate was much higher on the side of the CAM close to the

Fig. 5 | Migrasomes induce capillary formation and recruitment of monocytes. **a**, Purified migrasomes from CAM9d. Scale bars, 5 μm (top) and 500 nm (bottom). **b,c**, Newly formed capillaries on nylon mesh were visualized (**b**) (scale bars, 500 μm (left) and 50 μm (right)) and quantified (**c**). Error bar, \pm s.e.m.; $n = 15$ fields from three independent experiments; P values, two-tailed, unpaired t -test, $P < 0.0001$. **d**, Ex vivo sprouting assay were visualized 5 days after adding migrasome. Scale bars, 200 μm (top) and 120 μm (bottom). **e**, Cells from ex vivo sprouting assay were stained with indicated dye/antibody. Scale bar, 100 μm . **f,g**, Quantification of **d** in terms of EC tube length (**f**) and the total area of ECs emanating from CAM (**g**). Error bar, \pm s.e.m.; $n = 5$ (**f**) or 7 (**g**) CAM leaflets from five independent experiments; P values, two-tailed, unpaired t -test, $P < 0.0001$. **h**, Cells were stained with Lifeact and ASM1. Red arrowheads, filopodia of tip cells. Scale bar, 40 μm . **i**, Quantification of the numbers of filopodia from **h**. Error bar, \pm s.e.m.; $n = 16$ fields from five independent

experiments; $P < 0.0001$. **j**, Migrasomes were delivered to CAM9d. After 48 h, CAMs were visualized. Scale bar, 30 μm . Insert, enlarged region of interest (ROI). **k**, CAMs from **j** were quantified for the number of WGA^{high} cells. Error bar, \pm s.e.m.; $n = 15$ fields from three independent experiments; $P = 0.0057$. **l**, EC tube formation with or without migrasomes. Scale bar, 50 μm . **m**, EC tubes from **l** were quantified for mature tubes. Error bar, \pm s.e.m.; $n = 15$ fields from three independent experiments; $P < 0.0001$. **n**, Diagram of the transwell assay. **o**, Cells adhered to the underside of the transwell membrane were stained by DAPI. Scale bar, 30 μm . **p**, Migration indexes quantification using a two-tailed, unpaired t -test. Error bar, \pm s.e.m.; $n = 33$ fields from three independent experiments; NS (no significance, $P = 0.5165$), $P < 0.0001$. **q**, Migrasome stimulation triggers VEGFR2 and AKT activation. Source numerical data and unprocessed blots are available in source data.

migrasomes compared with the side without migrasomes (Extended Data Fig. 5a,b). Together, these data suggest that migrasomes can promote the proliferation and migration of ECs. This system also allows us to assess the role of migrasomes in EC sprouting. Two days after mounting, we clearly observed elongated filopodia on the tip cells (Extended Data Fig. 5a). This indicates that sprouting had occurred. Five days after adding agarose to the CAM, there were significantly more EC sprouting events and elongated filopodia on the tip cell marked by ASM1 and actin on the migrasome side than on the control side (Fig. 5h,i). Collectively, these data suggest that migrasomes promote the migration, proliferation and sprouting of ECs.

Migrasomes enhance EC tube formation and monocyte chemotaxis

To further verify the capacity of migrasomes to promote capillary formation, we carried out the EC tube formation assay, which is widely used to assess the differentiation and proliferation of ECs during angiogenesis. Similar to the in vivo result, we found that adding migrasomes significantly enhances tube formation (Fig. 5l,m). Consistent with this observation, we found that migrasomes can activate VEGFR2 signalling in vitro (Fig. 5q and Extended Data Fig. 6). We also tested the role of migrasomes in recruitment of monocytes in vitro by the transwell assay (Fig. 5n). We found that migrasomes markedly enhance the chemotaxis of WGA^{high} monocytes; in contrast, migrasomes only slightly enhance the chemotaxis of WGA^{low} cells (Fig. 5o,p). Put together, these data support a role for migrasomes in promoting capillary formation and monocyte recruitment.

Blocking migrasome formation impairs capillary formation

To further test the role of migrasomes in capillary formation, we performed RNA interference (RNAi) KD of *TSPAN4*, an essential gene for migrasome formation^{22,23}. We found that KD of *TSPAN4* significantly blocked migrasome formation and reduced capillary formation (Fig. 6a–e). This suggests that migrasomes do play important roles in capillary formation. Similarly, knocking down *TSPAN4* caused reduced

recruitment of monocytes (Fig. 6f,g). To distinguish the roles of *TSPAN4* from the role of migrasomes in angiogenesis, we carried out a rescue experiment in which we added migrasomes isolated from wild-type CAM to the place where the *TSPAN4* siRNAs were delivered. Addition of migrasomes successfully rescued monocyte recruitment and capillary formation (Fig. 6h,i and Extended Data Fig. 7e,f), which suggests that *TSPAN4* affects capillary formation by affecting migrasome formation.

To further support this observation, we established a protocol to knock out *TSPAN4* in the early stage of chicken embryonic development. Knockout of *TSPAN4* was achieved by using the clustered regularly interspaced short palindromic repeats (CRISPR)/Cas9 system to knock in mCherry at exon 5 of the chicken *TSPAN4* gene (Extended Data Fig. 8a). In brief, plasmids encoding guide RNAs (gRNAs) and Cas9 were injected into chick embryos at the gastrulating stage along with an mCherry knock-in plasmid. The knockout efficiency is indicated by mCherry expression, which occurs only in cells where *TSPAN4* has been successfully knocked out (Fig. 6j,k). This protocol worked well: we routinely achieved knockout in more than 70% of cells (Fig. 6l). We found that migrasome formation in *TSPAN4*-knockout CAM is significantly reduced (Fig. 6m,n). In addition, migrasome formation in vitro is reduced in monocytes isolated from *TSPAN4*-knockout CAM (Extended Data Fig. 8b). Moreover, in agreement with the RNAi KD experiment, both recruitment of monocytes and formation of capillaries are significantly reduced (Fig. 6o,p and Extended Data Fig. 8c,d). We also attempted to rescue the defects in *TSPAN4*-knockout CAM. The capillary formation defect is visible in CAM8d. Therefore, in the rescue experiment, we added migrasomes at 8 days and assessed the effects after 48 h. Unfortunately, knockout of *TSPAN4* causes embryo lethality at 9 days. Thus, despite our repeated efforts, we could not evaluate the rescue effect.

Migrasomes provide VEGFA and CXCL12 for angiogenesis

Finally, to investigate whether migrasomes affect angiogenesis through enrichment of VEGFA and/or CXCL12, we knocked down *VEGFA* and *CXCL12* successfully by RNAi (Extended Data Fig. 9a–c). We found that

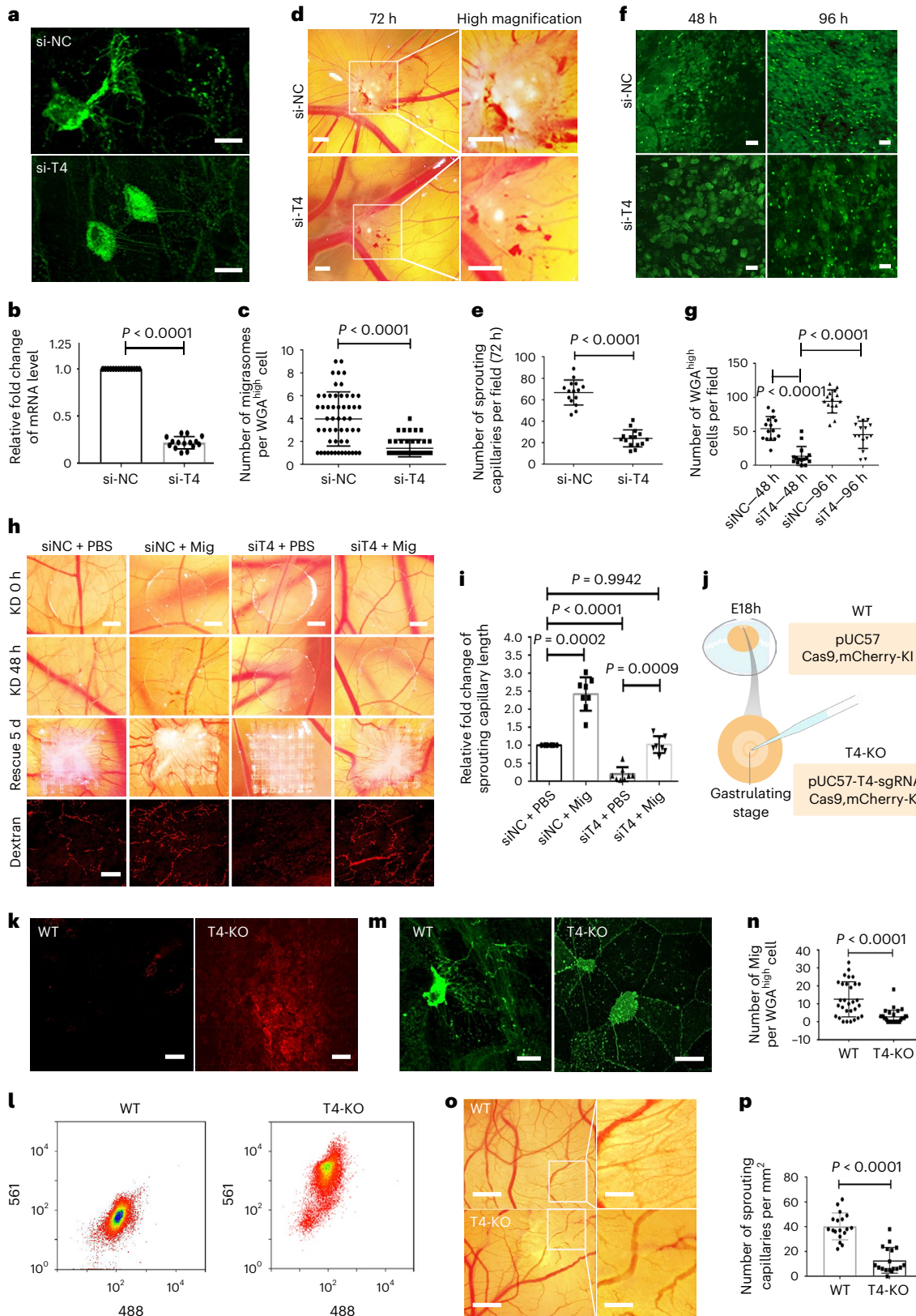
Fig. 6 | Blocking migrasome formation impairs capillary formation.

a, Confocal images of *TSPAN4* siRNA transfected CAM8d stained with WGA. Scale bar, 10 μm . **b,c**, Quantification of *TSPAN4*-KD efficiency or migrasome formation from **a**. Data are presented as mean \pm s.e.m.; $n = 15$ pieces (**b**) or 54 cells (**c**) from three independent experiments; P values, two-tailed, unpaired t -test, $P < 0.0001$. **d**, *TSPAN4* KD CAM8d visualized by stereomicroscopy. Right side shows enlarged ROI. Scale bar, 500 μm . **f**, *TSPAN4* KD CAM8d stained by WGA and visualized by confocal microscopy. Scale bar, 30 μm . **g,e**, Quantification of sprouting capillaries number or the number of WGA^{high} cells. Data are presented as mean \pm s.e.m.; $n = 15$ fields from three independent experiments; P values, two-tailed, unpaired t -test, $P < 0.0001$. **h**, Forty-eight hours after RNAi transfection, migrasomes were added to CAM on top of a nylon mesh. Five days later, CAMs were visualized by stereomicroscopy. Scale bar, 500 μm . Newly formed capillaries on the nylon mesh were visualized by Andor spinning disk microscopy. Scale bar, 50 μm . **i**, Post-treated CAMs from **h** were quantified for

newly formed capillaries. Data are presented as mean \pm s.e.m.; $n = 8$ fields from three independent experiments; P values, one-way ANOVA unpaired multiple comparisons, NS, no significance ($P = 0.9942$); $P = 0.0002$ (siNC + PBS versus siNC + migrasome); $P = 0.0009$ (si*TSPAN4* + PBS versus si*TSPAN4* + migrasome); $P < 0.0001$. **j**, Diagram of strategy for generating mosaic knockout chicken embryos. **k**, *TSPAN4*-KO efficiency monitored by expression of mCherry. Scale bar, 20 μm . **l**, *TSPAN4*-KO efficiency evaluated by flow cytometry. **m**, CAMs from **k–l** were stained for WGA and observed by spinning disk microscopy. Scale bar, 10 μm . **o**, CAMs from **k–l** were visualized by stereomicroscopy. Scale bar, 500 μm ; enlarged boxed areas, 200 μm . **n,p**, Migrasome generated by WGA^{high} cells from **m** or capillary formation from **o** were quantified. Data are presented as mean \pm s.e.m.; $n = 30$ (**n**) or 18 (**p**) fields from three independent experiments; P values, two-tailed, unpaired t -test, $P < 0.0001$. Source numerical data are available in source data.

KD of *VEGFA* or *CXCL12* significantly reduced capillary formation 48 h after adding RNAi (Fig. 7b,c and Extended Data Fig. 9d,e). At this point, we added isolated migrasomes from wild-type CAM and re-assessed the capillary formation after rescue. We found that adding migrasomes largely rescued capillary formation (Fig. 7a–c and Extended Data Fig. 9d,e).

Using a similar protocol, we tested the role of migrasomal CXCL12 in recruitment of monocytes. We found that CXCL12 is required for recruitment of monocytes, and adding migrasomes rescued the impaired monocyte recruitment in *CXCL12* KD CAM (Fig. 7d,e).



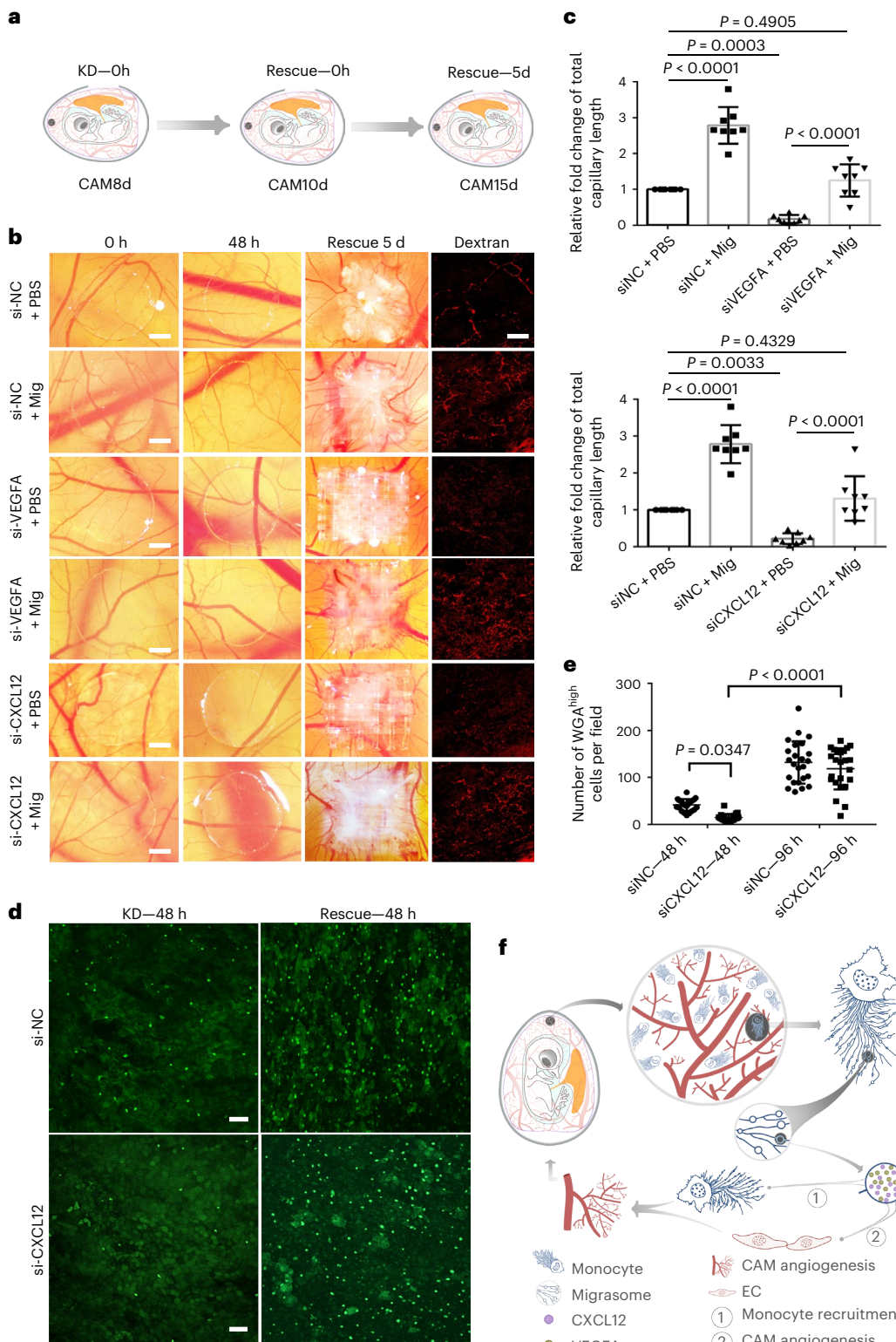


Fig. 7 | Migrasomes rescue capillary formation and monocyte recruitment defects in VEGFA-KD and CXCL12 KD CAM. **a**, Diagram showing the migrasome rescue assay after KD of VEGFA or CXCL12 in CAM. **b**, Forty-eight hours after RNAi transfection, migrasomes embedded in a collagen I–Matrigel matrix were added to CAM by nylon mesh assay. Five days later, CAMs were visualized by stereomicroscopy. Scale bar, 500 μ m. Newly formed capillaries on the nylon mesh were stained by dextran-FITC and visualized by Andor spinning disk microscopy; scale bar, 50 μ m. **c**, Post-treated CAMs from **b** were quantified for newly formed capillaries. Data are presented as mean \pm s.e.m.; $n = 8$ fields from three independent experiments; in siVEGFA group, P values were calculated using a one-way ANOVA unpaired multiple comparisons, NS (no significance, $P = 0.4905$), $P = 0.0003$, $P < 0.0001$; in siCXCL12 group, P values were calculated using a one-way ANOVA unpaired multiple comparisons, NS (no significance, $P = 0.4329$), $P = 0.0033$, $P < 0.0001$. **d**, CAMs from Extended Data Fig. 9d were stained with WGA and visualized by confocal microscopy. Scale bar, 50 μ m. **e**, CAMs from **d** were quantified for the number of WGA^{high} cells. Data are presented as mean \pm s.e.m.; $n = 22$ fields from three independent experiments; P values were calculated using a one-way ANOVA unpaired multiple comparisons, $P = 0.0347$; $P < 0.0001$. **f**, Model of the role of migrasomes from monocytes in angiogenesis during embryonic development. Source numerical data are available in source data.

one-way ANOVA unpaired multiple comparisons, NS (no significance, $P = 0.4905$), $P = 0.0003$, $P < 0.0001$; in siCXCL12 group, P values were calculated using a one-way ANOVA unpaired multiple comparisons, NS (no significance, $P = 0.4329$), $P = 0.0033$, $P < 0.0001$. **d**, CAMs from Extended Data Fig. 9d were stained with WGA and visualized by confocal microscopy. Scale bar, 50 μ m. **e**, CAMs from **d** were quantified for the number of WGA^{high} cells. Data are presented as mean \pm s.e.m.; $n = 22$ fields from three independent experiments; P values were calculated using a one-way ANOVA unpaired multiple comparisons, $P = 0.0347$; $P < 0.0001$. **f**, Model of the role of migrasomes from monocytes in angiogenesis during embryonic development. Source numerical data are available in source data.

Discussion

In this study, we found that migrasomes are generated by monocytes/macrophages in the CAM during chicken embryonic development. We further demonstrated that migrasomes play an important role in angiogenesis by delivering angiogenic factors such as VEGFA and CXCL12 to the area of capillary formation, thus creating a favourable microenvironment for angiogenesis. We also found that monocytes can recruit more monocytes via migrasomes through CXCL12-mediated chemotaxis. This creates a positive feedback loop, which can sustain the rapid capillary formation in CAM.

It is well established that VEGF can be sequestered by the extracellular matrix (ECM) near VEGF-secreting cells, which restricts the diffusion of VEGF and creates a signalling pattern¹¹. We speculate that, beside this well-established mechanism, migrasomes may represent an additional mechanistic layer, which can generate signal patterns and gradients. Using migrasomes as the signal source to guide angiogenesis has multiple advantages. Firstly, for many angiogenic factors that do not bind to ECM, migrasomes provide a mechanism for creating spatial and temporal signal patterns. Secondly, multiple different kinds of angiogenic factors can be packed into the same migrosome. These factors, which may contribute to angiogenesis through different yet complementary mechanisms, can undergo synchronized release, thus ensuring the spatial and temporal coordination of diverse regulatory mechanisms for angiogenesis. Finally, the release of angiogenic factors from migrasomes requires the rupture or leakage of migrasomes. This creates a latency effect and provides more opportunity to fine-tune the formation of signal patterns.

Our work highlights the importance of monocytes in angiogenesis during embryonic development. On the basis of these finding, we propose a ‘vanguard’ model for angiogenesis, in which migratory monocytes serve as forerunners to prepare a favourable microenvironment for angiogenesis in advance of capillary formation (Fig. 7f).

Beside angiogenesis during embryonic development, the involvement of monocytes in physiological homeostasis of adult tissue and in pathological conditions is well documented^{33,34}. For example, in injury-induced angiogenesis and tumour angiogenesis, monocyte-derived macrophages and tumour-associated macrophages have been shown to promote angiogenesis by secretion of VEGFA^{35–38}. Therefore, it is possible that migrosome formation is also involved in these processes.

In addition to angiogenesis, monocytes and macrophages carry out a complicated set of functions in different biological settings, including lymphangiogenesis, tissue remodelling, and inflammatory and immune responses^{35,39–42}. Many of these functions depend on secretion of cytokines, chemokines and growth factors; moreover, many of these biological processes require the spatial and temporal coordination and integration of a complex set of secreted ligands^{43–45}. Thus, we speculate that migrasomes may also play important roles in these processes.

Online content

Any methods, additional references, Nature Portfolio reporting summaries, source data, extended data, supplementary information, acknowledgements, peer review information; details of author contributions and competing interests; and statements of data and code availability are available at <https://doi.org/10.1038/s41556-022-01026-3>.

References

1. Majesky, M. W. Vascular development. *Arterioscler. Thromb. Vasc. Biol.* **38**, e17–e24 (2018).
2. Chung, A. S. & Ferrara, N. Developmental and pathological angiogenesis. *Annu. Rev. Cell Dev. Biol.* **27**, 563–584 (2011).
3. Distler, J. H. et al. Angiogenic and angiostatic factors in the molecular control of angiogenesis. *Q. J. Nucl. Med.* **47**, 149–161 (2003).
4. Risau, W. & Flamme, I. Vasculogenesis. *Annu. Rev. Cell Dev. Biol.* **11**, 73–91 (1995).
5. Karamysheva, A. F. Mechanisms of angiogenesis. *Biochem.* **73**, 751–762 (2008).
6. Melincovici, C. S. et al. Vascular endothelial growth factor (VEGF)—key factor in normal and pathological angiogenesis. *Rom. J. Morphol. Embryol.* **59**, 455–467 (2018).
7. Ribatti, D. The discovery of the fundamental role of VEGF in the development of the vascular system. *Mech. Dev.* **160**, 103579 (2019).
8. Takahashi, H. & Shibuya, M. The vascular endothelial growth factor (VEGF)/VEGF receptor system and its role under physiological and pathological conditions. *Clin. Sci.* **109**, 227–241 (2005).
9. Apte, R. S., Chen, D. S. & Ferrara, N. VEGF in signaling and disease: beyond discovery and development. *Cell* **176**, 1248–1264 (2019).
10. Pardali, E., Goumans, M. J. & ten Dijke, P. Signaling by members of the TGF-beta family in vascular morphogenesis and disease. *Trends Cell Biol.* **20**, 556–567 (2010).
11. Vempati, P., Popel, A. S. & Mac Gabhann, F. Extracellular regulation of VEGF: isoforms, proteolysis, and vascular patterning. *Cytokine Growth Factor Rev.* **25**, 1–19 (2014).
12. Poltorak, Z. et al. VEGF145, a secreted vascular endothelial growth factor isoform that binds to extracellular matrix. *J. Biol. Chem.* **272**, 7151–7158 (1997).
13. Vempati, P., Popel, A. S. & Mac Gabhann, F. Formation of VEGF isoform-specific spatial distributions governing angiogenesis: computational analysis. *BMC Syst. Biol.* **5**, 59 (2011).
14. Poltorak, Z., Cohen, T. & Neufeld, G. The VEGF splice variants: properties, receptors, and usage for the treatment of ischemic diseases. *Herz* **25**, 126–129 (2000).
15. Qian, B. Z. & Pollard, J. W. Macrophage diversity enhances tumor progression and metastasis. *Cell* **141**, 39–51 (2010).
16. Leek, R. D. et al. Association of macrophage infiltration with angiogenesis and prognosis in invasive breast carcinoma. *Cancer Res.* **56**, 4625–4629 (1996).
17. Ruhrberg, C. & De Palma, M. A double agent in cancer: deciphering macrophage roles in human tumors. *Nat. Med.* **16**, 861–862 (2010).
18. Priceman, S. J. et al. Targeting distinct tumor-infiltrating myeloid cells by inhibiting CSF-1 receptor: combating tumor evasion of antiangiogenic therapy. *Blood* **115**, 1461–1471 (2010).
19. Stockmann, C. et al. Deletion of vascular endothelial growth factor in myeloid cells accelerates tumorigenesis. *Nature* **456**, 814–818 (2008).
20. Fantin, A. et al. Tissue macrophages act as cellular chaperones for vascular anastomosis downstream of VEGF-mediated endothelial tip cell induction. *Blood* **116**, 829–840 (2010).
21. Cattin, A. L. et al. Macrophage-induced blood vessels guide Schwann cell-mediated regeneration of peripheral nerves. *Cell* **162**, 1127–1139 (2015).
22. Ma, L. et al. Discovery of the migrosome, an organelle mediating release of cytoplasmic contents during cell migration. *Cell Res.* **25**, 24–38 (2015).
23. Huang, Y. et al. Migrosome formation is mediated by assembly of micron-scale tetraspanin macromolecular domains. *Nat. Cell Biol.* **21**, 991–1002 (2019).
24. Wu, D. et al. Pairing of integrins with ECM proteins determines migrosome formation. *Cell Res.* **27**, 1397–1400 (2017).
25. Jiang, D. et al. Migrasomes provide regional cues for organ morphogenesis during zebrafish gastrulation. *Nat. Cell Biol.* **21**, 966–977 (2019).
26. Chen, L., Ma, L. & Yu, L. WGA is a probe for migrasomes. *Cell Discov.* **5**, 13 (2019).

27. Grad, E. et al. The role of monocyte subpopulations in vascular injury following partial and transient depletion. *Drug Deliv. Transl. Res.* **8**, 945–953 (2018).
28. Bruhl, H. et al. Targeting of Gr-1⁺,CCR2⁺ monocytes in collagen-induced arthritis. *Arthritis Rheum.* **56**, 2975–2985 (2007).
29. Udalova, I. A., Mantovani, A. & Feldmann, M. Macrophage heterogeneity in the context of rheumatoid arthritis. *Nat. Rev. Rheumatol.* **12**, 472–485 (2016).
30. Jaipersad, A. S., Lip, G. Y., Silverman, S. & Shantsila, E. The role of monocytes in angiogenesis and atherosclerosis. *J. Am. Coll. Cardiol.* **63**, 1–11 (2014).
31. Moldovan, L. & Moldovan, N. I. Role of monocytes and macrophages in angiogenesis. *EXS* **94**, 127–146 (2005).
32. Zhao, X. et al. Identification of markers for migrasome detection. *Cell Disco.* **5**, 27 (2019).
33. Sica, A., Erreni, M., Allavena, P. & Porta, C. Macrophage polarization in pathology. *Cell. Mol. Life Sci.* **72**, 4111–4126 (2015).
34. Ginhoux, F. & Jung, S. Monocytes and macrophages: developmental pathways and tissue homeostasis. *Nat. Rev. Immunol.* **14**, 392–404 (2014).
35. Riabov, V. et al. Role of tumor associated macrophages in tumor angiogenesis and lymphangiogenesis. *Front Physiol.* **5**, 75 (2014).
36. Vannella, K. M. & Wynn, T. A. Mechanisms of organ injury and repair by macrophages. *Annu. Rev. Physiol.* **79**, 593–617 (2017).
37. Allavena, P., Sica, A., Solinas, G., Porta, C. & Mantovani, A. The inflammatory micro-environment in tumor progression: the role of tumor-associated macrophages. *Crit. Rev. Oncol. Hematol.* **66**, 1–9 (2008).
38. Wyckoff, J. B. et al. Direct visualization of macrophage-assisted tumor cell intravasation in mammary tumors. *Cancer Res.* **67**, 2649–2656 (2007).
39. Das, A. et al. Monocyte and macrophage plasticity in tissue repair and regeneration. *Am. J. Pathol.* **185**, 2596–2606 (2015).
40. Wynn, T. A. & Vannella, K. M. Macrophages in tissue repair, regeneration, and fibrosis. *Immunity* **44**, 450–462 (2016).
41. Murray, P. J. Immune regulation by monocytes. *Semin. Immunol.* **35**, 12–18 (2018).
42. Shi, C. & Pamer, E. G. Monocyte recruitment during infection and inflammation. *Nat. Rev. Immunol.* **11**, 762–774 (2011).
43. Pakshir, P. & Hinz, B. The big five in fibrosis: macrophages, myofibroblasts, matrix, mechanics, and miscommunication. *Matrix Biol.* **68–69**, 81–93 (2018).
44. Evans, M. A. et al. Macrophage-mediated delivery of light activated nitric oxide prodrugs with spatial, temporal and concentration control. *Chem. Sci.* **9**, 3729–3741 (2018).
45. Theoret, C. L., Barber, S. M. & Gordon, J. R. Temporal localization of immunoreactive transforming growth factor beta1 in normal equine skin and in full-thickness dermal wounds. *Vet. Surg.* **31**, 274–280 (2002).

Publisher's note Springer Nature remains neutral with regard to jurisdictional claims in published maps and institutional affiliations.

Springer Nature or its licensor (e.g. a society or other partner) holds exclusive rights to this article under a publishing agreement with the author(s) or other rightsholder(s); author self-archiving of the accepted manuscript version of this article is solely governed by the terms of such publishing agreement and applicable law.

© The Author(s), under exclusive licence to Springer Nature Limited 2022

Methods

The study was conducted according to the guidelines of the Academic Integrity and Ethics committee of Tsinghua University.

Cultivation of SPF chick eggs

Fertilized specific-pathogen-free (SPF) eggs (variety, White Leghorn; cleanliness, SPF) were bought from Beijing Boehringer Ingelheim Vital Biotechnology. The eggs were incubated in a hatching incubator at 37.5 °C with 60–70% humidity. Eggs were turned every 5 min. All SPF chick embryos used in the study were assessed from embryonic 18 h to embryonic day 15. All animal experiments were conducted according to the guidelines of the Animal Care and Use Committee of Tsinghua University.

Reagents

The antibody against VEGFA was generated by ABclonal Technology (Co. WG-04988). The antibody against CXCL12 was from LSBio (Co. LS-B943-100). The anti-Integrin α 5 antibody was from Cell Signaling Technology (4705S). The antibody against GAPDH was from Protein-tech (60060004-1-IG). The antibody against NDST was from Santa Cruz Biotechnology (sc-374529). The antibody against CPQ was generated by Sigma (HPA023235). The KUL01 antibody was from Southern-Biotech (8420-09). The antibody against CD115 (CSF1R) and the Alexa Fluor-tagged antibodies CD115-Alexa488 and CD115-Alexa647 were from Bio-Rad (MCA5956GA, MCA5956GA488 and MCA5956GA647). The antibody against TSG101 was from Abcam (ab125011). The antibody against Calnexin was from Abcam (ab22595). The antibody against CCR2 was from Thermo Fisher (Thermo PA5-23037). The antibody against VEGFR2 was from Thermo Fisher (MA5-15157). The antibody against Phospho-VEGFR2 was from CST (2474T). The antibody against AKT was from CST (no. 9272). The antibody against Phospho-AKT was from CST (no. 9271).

WGA was from Life Technologies (W11261). CellTracker Red CMTPX was from Invitrogen Life Technologies (C34552). GM-CSF was from PeproTech (315-03). Lipofectamine 3000 transfection reagent and P3000 reagent were from Invitrogen Life Technologies (L3000015). Matrigel Basement Membrane Matrix was from Corning (356234). Dextran was from Sigma-Aldrich (46945-100MG-F). PBS liposomes and clodronate liposomes were from LIPOSOMA research (C-005, P-005). Control liposomes and alendronate liposomes were from FormuMax (F70103A-A, FormuMax). Low-melting-point agarose II was from AMRESCO (0815-25G). Collagen I coating solution was from Sigma-Aldrich (122-20). The recombinant human VEGF165 was from PeproTech (100-20, PeproTech). The nylon mesh was from SK (TS207-050, SK, pore size 300 μ m).

PBS was from Cytiva HyClone (SH30256.01). ECM was from ScienCell Research Laboratories (1001). 0.25% Trypsin + 0.02% EDTA solution was from Cienry (CR-25200). Penicillin-streptomycin solution was from GENOM (GNM15140). GlutaMAX I (100 \times) was from Gibco (35050-061); 4% paraformaldehyde was from Dingguo Changsheng Biotechnology (ar-0211).

Collagenase type II powder was from Gibco (17101-015). Lysosome isolation kit was from Sigma-Aldrich (LYSISO1-1KT).

RealStar green power mixture (2 \times) was from Gibco (A311-01). TaKaRa MiniBEST Universal RNA Extraction kit was from TaKaRa (9767). Endofree plasmid Midi kit was from CWBIO (CW2105S). TIANgel Midi Purification kit was from Tiangen (DP209-02).

Cell culture and treatment

Human umbilical vein endothelial cells (HUVECs) were grown in ECM (ScienCell) and used between passages 3 and 5. Cells were grown at 37 °C in a humidified incubator with 5% CO₂. WGA^{high} cells were cultured in RPMI 1640 medium (Gibco) supplemented with 10% v/v foetal calf serum (Sigma-Aldrich), 2 mM L-glutamine and 1% v/v (500 U ml⁻¹) penicillin-streptomycin. Cells were grown at 37 °C in a humidified incubator with 5% CO₂.

Migrasome purification

Migrasome purification was performed by iodixanol sucrose density-gradient centrifugation using an Optiprep kit (LYSISO1, Sigma-Aldrich). CAMs were isolated from E9d chicken embryos (approximately 8 embryos for the rescue experiments and 30 embryos for Q-MS analysis), then subjected to mechanical mincing. The chopped-up CAMs were then treated with collagenase II and trypsin. The samples were centrifuged at 1,000g for 5 min at 4 °C to remove the cell bodies, followed by 4,000g for 20 min at 4 °C to remove the cell fragments, and finally at 20,000g for 20 min at 4 °C. The pellet containing the crude migrasome fraction was re-suspended and lysed in extraction buffer (Sigma-Aldrich) and then fractionated at 150,000g for 4 h at 4 °C in a multi-step Optiprep dilution gradient. The gradient was: 3%, 5%, 8%, 12%, 16%, 19% (sample), 22.5% and 27%. Fractions were collected and added to 500 μ l PBS. Centrifugation was then performed at 20,000g for 30 min at 4 °C. The pellet was collected, washed once with PBS and centrifuged at 4 °C, 2,000g for 10 min. The supernatant was collected and centrifuged at 4 °C, 20,000g for 30 min to obtain migrasomes for TEM observation and injection into embryos.

Tube formation assay

HUVECs were cultured for 24 h then used for the tube formation assay. The cells were then synchronized by incubating them in ECM containing 0.1% FBS for 12 h. The assay was then performed according to the description in the manual (BD Biosciences). Briefly, six-well plates were coated with Matrigel Basement Membrane Matrix (BD Biosciences; diluted in basal ECM at a ratio of 1:1; 500 μ l mixture per well) and incubated at 37 °C for 30 min to allow gelation. HUVECs were plated at a density of 2 \times 10⁶ cells per well. Cells were incubated at 37 °C with 5% CO₂ within 24 h, and pictures were captured with a light microscope (Olympus).

Observation of migrasome formation in CAM in vivo

Firstly, a square hole (about 1 \times 1 cm) was cut in the eggshell. Secondly, WGA was diluted in 1×PBS (1:500, 200 μ l 1×PBS), and then this mixture was added to the top of the CAM. After staining for 20 min at 37.5 °C in a humidified incubator with 70% humidity, the egg was placed on a holder with the hole in direct contact with a cover glass, so that the weight of the egg held the CAM in tight contact with the cover glass. Last, the CAM was visualized under a Nikon A1 FV3000 confocal microscope and a Dragonfly Andor spinning disk confocal microscopy.

Migrasome delivery by Matrigel or agarose

Fertilized chick eggs were incubated at 37.5 °C for 9 days. Then the E8d eggs were windowed. Five microlitres (20 μ g μ l⁻¹, 100 μ g) of migrasome sediment were embedded in 3 μ l low-melting-point agarose or 3 μ l Matrigel. After the mixture solidified, it was placed onto the CAM. Forty-eight hours later, images were captured by a Leica EZ4W stereomicroscope.

RNAi treatment of CAM and rescue by migrasome delivery

Fertilized chick eggs were incubated at 37.5 °C for 8 days. Then the E8d eggs were windowed and the CAM tissue was transfected with 2.5 μ g siRNA for target genes (*TSPAN4*, *VEGFA*, *CXCL12*, GenePharma) with Lipofectamine 3000 (Thermo Fisher Scientific, 100022052) and P3000 (Thermo Fisher Scientific, 100022058) according to the manufacturer's instructions. A pair of platinum electrodes (Nepagene) was used for electroporation. Electroporation (five pulses of 50 ms duration at 20 mV) was used to improve the transfection efficiency. In all siRNA experiments, siNC (GenePharma) was used as the control. The KD efficiency of the target gene *TSPAN4* was confirmed by quantitative real-time PCR (qPCR) analysis. After the target gene was knocked down successfully, 5 μ l (20 μ g μ l⁻¹, 100 μ g) of migrasome sediment were embedded in 3 μ l of low-melting-point agarose. After the mixture solidified, it was placed onto the CAM.

Flow cytometry

The mAbs used for flow cytometry are listed in STAR METHODS. Isolation of monocytes was performed by flow cytometry using anti-CD115 antibody. For isolation of WGA^{high} cells, briefly, CAMs were stained by WGA in vivo, then treated with collagenase II and trypsin. After removing the red blood cells, the residual cells (about 2×10^7) were sorted by FACS. For isolation of CD115⁺ cells, cells were isolated from CAMs as described above, then incubated with anti-CD115 antibody (5×10^6 cells in $600 \mu\text{l}$ 1× PBS, 1:10, 37 °C, 20 min) and sorted by FACS. To estimate the efficiency of *TSPAN4* knockout in CAM9d, mCherry-positive cells were counted by flow cytometry.

TEM

CAMs isolated from 9-day-old chick embryos were fixed with 2.5% glutaraldehyde + 2.0% paraformaldehyde diluted in 0.1 M phosphate buffer (0.1 M Na₂HPO₄.12H₂O and 0.1 M NaH₂PO₄.2H₂O, pH 7.2). The CAMs were kept at room temperature for 2 h and then at 4 °C overnight. After three 10 min washes with 0.1 M PB, the CAMs were treated with 1.5% K₃Fe(CN)₆ + 1% OsO₄ (mixed before use) and kept at 4 °C for 1.5 h. The CAMs were washed three times with ddH₂O (10 min each wash), and then treated with 1% uranyl acetate in water and kept at 4 °C overnight. After three 15 min washes in ddH₂O, the samples were dehydrated in ethanol (50%, 70%, 80%, 90%, 100%, 100% and 100%; 15 min each), then treated with 100% ethanol:100% acetone at a 1:1 ratio for 8 min, and finally with 100% acetone for 8 min. The CAMs were infiltrated with PON812 resin as follows: 1:1 resin:acetone, 2 h at room temperature; 2:1 resin:acetone, 2 h at room temperature; 3:1 resin:acetone, 2 h at room temperature; resin alone, overnight; and resin alone, 2 h. Each CAM was then placed in the correct orientation on a 3.5 mm culture dish and a capsule filled with resin was placed over the CAM. The resin was polymerized at 37 °C for 8 h, 45 °C for 24 h and 60 °C for 12 h. Sections (70 nm) were cut with a Leica EM UC7 microtome and then stained with uranyl acetate and lead citrate. Images were obtained with a H-7650B TEM at 50–70 kV.

Imaging

To acquire two-dimensional images of vessel sprouting in CAMs in vivo, migrasomes or siRNA were added at the desired embryonic stage, then the CAMs were imaged by a Leica EZ4W stereomicroscope. Time-lapse multiple-view z-stack images (4D) of WGA^{high} cells were acquired for statistical analysis of migration and migrosome production. *TSPAN4*-KD, *TSPAN4*-KO, anti-CCR2 or clodronate/alendronate treatments were applied after windowing at the desired embryonic stage. Then the egg was placed on a holder with the window directly touching a cover glass, so that the weight of the egg kept the CAM in contact with the cover glass. The CAM was imaged by Olympus FV1000 confocal microscopy, Nikon A1 confocal microscopy or spinning disk microscopy (Andor Dragonfly).

Image processing

All of the time-lapse multiple-view z-stack embryo images (4D images) were processed using Imaris software 8.1.4 and 9.5.0 (Bitplane AG). Images were processed by ImageJ v1.8.0.112 and Nikon NIS-Elements to quantify the fluorescence intensity to assess the number of WGA^{high} cells, the number of sprouting capillaries or the density of sprouting capillaries. Amira 6.0.0 software was used to reconstruct the 3D migrosome structure from FIB-SEM images. To determine the cell migration speed, time-lapse images were acquired by Nikon A1 and analysed using Imaris software 8.1.4 and 9.5.0. Flow cytometry data were acquired by MoFlo Astrios EQ or MoFlo XDP (beckMan) and analysed using CytoFLEX S or CytoFLeXL X.

TMT Q-MS analysis

First of all, proteins either from migrasomes (case) or from cell bodies (control) were prepared using 8 M urea in PBS (Wisent) containing

protease inhibitor cocktail. Second, all samples were sonicated for 2 min and centrifuged, and the supernatant was carefully separated. Protein concentrations were analysed using the BCA protein assay kit. Third, in-solution digestion was performed. A total of 100 µg of protein extracted from each sample was reduced with 5 mM dithiothreitol at room temperature and alkylated with 12.5 mM iodoacetamide in the dark at room temperature. Then, the mixture was diluted to 1.5 M urea with PBS and the proteins were digested with trypsin (Promega) at 37 °C overnight. Fourth, the tryptic peptides were desalted using Sep-Pak desalting columns (Waters), and then the desalted peptides were labelled with 15 µl TMT 10-PLEX reagents (Thermo Fisher Scientific). Three repeats in the control group were marked as 126, 126N and 127C. Three repeats in the case group were marked as 128C, 129N and 129C. These combined TMT-labelled peptides were desalted by Sep-Pak columns and separated with a UPLC 3000 system (Thermo Fisher Scientific) with an XBridgeTM BEH300 C18 column (Waters) at a flow rate of 1 ml min⁻¹. The mobile phase A was H₂O (pH 10) and the mobile phase B was 98% acetonitrile (pH 10). Peptides were separated with a gradient elution consisting of an increase from 8% to 18% phase B for 30 min, followed by an increase from 18% to 32% phase B for 22 min. Forty-eight fractions were dried by speedvac and recombined to 12 fractions. The fractions were dissolved in 20 µl of 0.1% (v/v) formic acid and analysed by liquid chromatography–mass spectrometry. Spectra from the mass spectrometer were searched against the UniProt *Gallus gallus* database using the SEQUEST search engine of Proteome Discoverer software (version 2.3). The identified proteins were quality monitored, and each protein with more than five points and with a specific peptide segment number greater than two was judged to be credible and was carried forward for the subsequent quantitative analysis. For the results of the peptide segment search, X_{corr} needed to be higher than 2.5 for the peptide segment to be judged as credible.

qPCR

To avoid contamination, all RNA-associated experiments were conducted in a molecular biology laboratory that is specifically designed for clinical diagnosis using molecular techniques, and which includes separate laboratories dedicated to performing each step of the procedure. Total RNA was isolated from CAM tissues with a TaKaRa MiniBEST Universal RNA Extraction Kit (Clontech TaKaRa, cat. no. 9796). Complementary DNA was synthesized from 2 µg total RNA using a reverse transcription kit (Promega) according to the manufacturer's instructions. Total RNA was isolated from cells with TRIzol reagent (Tiangen). qPCR was performed with the Roche LightCycler 480 II System (Roche) using SYBR green reaction mixture (GenStar, cat. no. A311-101) according to the manufacturer's instructions. GAPDH and ACTB were used as internal controls for messenger RNA quantification. *TSPAN4*, VEGFA and CXCL12 primers were acquired from Primer-Blast and are listed in STAR METHODS.

Western blotting

Whole-cell extracts or migrosome extracts were isolated from E9.5 chick embryos using RIPA buffer (50 mM Tris-HCl pH 8.0, 100 mM NaCl, 1% Triton X-100, 1% sodium deoxycholate, 0.1% SDS and 5 mM EDTA) or 2% SDS in 1× TBS complemented with protease inhibitors (complete protease inhibitor cocktail tablets, Roche). After determining the protein concentration of each sample using the BCA kit (Bio-Rad), 40 µg of lysate was resolved on 10% SDS-PAGE gels (Invitrogen) and transferred onto PVDF membranes (Amersham). Blots were then blocked with 5% milk in 1× PBS for 1 h at room temperature, followed by incubation with antibodies against Integrin α5/NDST1/CPQ/Calnexin/Tsg101/GAPDH/VEGFA/CXCL12/Alix/VEGFA/CXCL12/VEGFR2/phospho-VEGFR2/AKT/phospho-AKT at 4 °C overnight. Binding of HRP-conjugated secondary antibodies was subsequently visualized on the ChemiDoc MP Imaging System (Bio-Rad).

Immunofluorescence

For immunofluorescent detection of VEGFA or CXCL12 in migrasomes, monocytes were isolated from CAM, then cultured on galectin-coated chambers and treated by GM-CSF for about 12 h. The monocytes were stained by WGA488 (1:2,000) at 37 °C for 10 min, then washed with PBS, fixed in 4% paraformaldehyde and permeabilized for 10 min with 0.3% Triton X-100 in 1× PBS. The monocytes were then blocked with 5% milk in 1× PBS for 1 h at room temperature and incubated with anti-VEGFA or CXCL12 antibody at 4 °C overnight. After that, the cells were washed three times with 1× TBST, then incubated with Alexa 561-conjugated IgG antibody (Sigma) for 1 h at room temperature. The cells were finally washed with 1× TBST, and visualized under a Nikon A1 confocal microscope. For immunofluorescence imaging of CSF1R and KUL01 in CAM, E9d CAMs were isolated. Approximately 1 cm² of CAM was cut and incubated in diluted WGA buffer (1 µl WGA in 500 µl 1× PBS) at 37 °C for 20 min. Then the CAM was washed with 1× PBS, fixed in 4% paraformaldehyde for 2 h and permeabilized for 2 h with 0.3% Triton X-100 in 1× PBS. After permeabilization, the CAM was blocked with 5% BSA in 1× PBS for 6 h at room temperature and incubated with anti-CSF1R or KUL01 antibody at 4 °C overnight. After that, the CAM was washed three times with 1× TBST and incubated with Alexa 561-conjugated IgG antibody (Sigma) for 1 h at room temperature. The CAM was finally washed with 1× TBST and coated on SuperFrost Plus microscope slides by ProLong TM Diamond Anti-fade Mountant (P36970, Thermo Fisher Scientific). Co-localization of WGA^{high} signal and CSF1R or KUL01 was visualized with a Nikon A1 confocal microscope.

Yeast phagocytosis by monocytes after GM-CSF stimulation

Monocytes from CAM9d were sorted by FACS after incubation with anti-CD115 antibody (5 × 10⁶ cells in 600 µl 1× PBS, 1:10, 37 °C, 20 min). Then monocytes (1 × 10⁶) were cultured in chambers coated with 10% w/v gelatin solution. After that, monocytes were stimulated by GM-CSF (final concentration about 20 ng µl⁻¹, no. 315-03, Pepro-Tech) according to the manufacturer's instructions and stained by WGA (1:2,000, 10 min, 37 °C). Yeast cells (strain BY4741, 1 × 10⁷) were stained by CellTracker Red CMTPX (C34552, Thermo Fisher Scientific, 1:50,000, 95 °C, 30 min) and added to the chamber. Seventy-two hours later, images were acquired by spinning disk microscopy (Andor Dragonfly).

Monocyte depletion by clodronate liposomes

When chick eggs had developed to embryonic day 6, they were windowed and 2 µl clodronate liposomes or PBS liposomes (Liposoma BV) were microinjected into a vein in the CAM. After 48 h, 7.5 µl clodronate liposomes or PBS liposomes were microinjected into a vein of CAM. Then the windows were sealed by Parafilm and the eggs were incubated at 37.5 °C with 60% humidity. The CAMs were imaged by a Leica EZ4W stereomicroscope.

Monocyte depletion by alendronate liposomes

Chick eggs at embryonic day 6 were windowed and 0.6 µl alendronate liposomes or control liposomes (F70103A-A, FormuMax) were microinjected into a vein in the CAM. After 48 h, 2.3 µl alendronate liposomes or control liposomes (F70103A-A, FormuMax) were microinjected into a vein in the CAM. Sealing, incubation and imaging was carried out as described for clodronate liposomes.

Monocyte depletion by anti-CCR2

Chick eggs at embryonic day 6 were windowed and 0.6 µl anti-CCR2 (1 µg µl⁻¹, Thermo PA5-23037) or anti-IgG were microinjected into a vein in the CAM. After 24 h, 1.2 µl anti-CCR2 or anti-IgG were microinjected into a vein in the CAM. Then the windows were sealed by Parafilm and incubated at 37.5 °C with 60% humidity for another 24 h. The CAMs were imaged by a Leica EZ4W stereomicroscope.

Dextran staining of the blood vessel system

Chick eggs (E9d) were windowed. Twenty microlitres dextran (46945-100MG-F, 2 µg µl⁻¹) was microinjected into the vein system. Images were immediately captured by an FV3000 Olympus confocal microscope.

Monocyte tracing

Chick eggs (E9d) were windowed, and 20 µl CD115 (MCA5956GA488) were microinjected into the vein system. Ten minutes, 30 min or 120 min later, images were captured by FV3000 Olympus confocal microscopy.

Transwell chemotaxis assay

Transwell chemotaxis assays were performed with 12-well transwell plates. WGA^{high} or WGA^{low} cells were isolated by FACS after WGA staining. WGA^{high} or WGA^{low} cells were seeded in the upper chambers of the 12-well plate at 0.5 × 10⁶ cells ml⁻¹ in RPMI 1640 medium (Gibco) supplemented with 10% v/v foetal calf serum (Sigma-Aldrich), 2 mM L-glutamine and 1% v/v (500 U ml⁻¹) penicillin-streptomycin. Generally, 12-well plates employed 1.5 ml of this RPMI 1640 medium in the lower chamber and 500 µl in the upper chamber. To identify the chemotaxis response of WGA^{high} or WGA^{low} cells to migrasomes, 15 µg migrasomes (1.5 µl of 10 µg µl⁻¹ migrasomes in 1× PBS) were placed in the lower chambers as the case group and 1.5 µl 1× PBS were added in the lower chambers as the negative-control group. The plates were then incubated for 6 h. The upper chambers were removed and the cells coating the top side of the polycarbonate membranes (Corning) were thoroughly removed with swabs. Then the polycarbonate membranes were cut off, washed with 1× PBS, fixed in 4% paraformaldehyde for 30 min and stained by 4,6-diamidino-2-phenylindole (DAPI; 1 µg µl⁻¹, 1:1,000) for 15 min. Lastly, the polycarbonate membranes were coated on SuperFrost Plus microscope slides with ProLong TM Diamond Anti-fade Mountant (P36970, Thermo Fisher Scientific). The number of migrated cells adhered to the underside of the polycarbonate membrane was visualized and counted by Nikon A1 confocal microscopy.

VEGFR2 activation by EC chemotaxis assay

ECs were cultured in 0.1% FBS ECM and 1% v/v (500 U ml⁻¹) penicillin-streptomycin (ScienCell) for 24 h. ECs were seeded in six-well transwell plates at 2.0 × 10⁶ cells ml⁻¹ in the upper compartment of a Boyden chamber containing gelatin-coated PVP-free polycarbonate filters (8 µm pore size) in ECM (ScienCell) supplemented with 0.1% v/v foetal calf serum (ScienCell) and 1% v/v (500 U ml⁻¹) penicillin-streptomycin. A total of 50 ng ml⁻¹ of VEGF165 (PeproTech) or 10 µg µl⁻¹ migrasomes dissolved in 0.1% FBS ECM with 1% v/v (500 U ml⁻¹) penicillin-streptomycin placed in the lower compartment.

After 24 h of incubation at 37 °C, cells that migrated to the lower part of the filter were collected for western blot to detect the phosphorylation of VEGFR2 and so on.

Generation of T4-KO-mCherry-KI embryos by the CRISPR system

A CRISPR/Cas9-based gene editing strategy was used to achieve *TSPAN4* gene knockout in chick embryos. A gRNA coding sequence was cloned into pUC57 vector (Addgene 55132) as the gRNA plasmid backbone, and the empty pUC57 vector was constructed as negative control that did not contain a single guide RNA (sgRNA) sequence. An sgRNA (*TSPAN4-Gallus*-gRNA1-Bsa1-F, 5'-TAGGGAAAGGTGAAGACAAACATT-3'; *TSPAN4-Gallus*-gRNA1-Bsa1-R, 5'-AAACAATGTTGTCTAACCTTC-3') was then designed to target exon 5 of chick *TSPAN4*. The sgRNA was inserted into the sgRNA expression cassettes of the pUC57 vector under control of the T7 promoter. Then the vector was introduced by chemical transformation into competent *E. coli* Top10 for cloning purposes using a kanamycin selectable marker.

To evaluate the *TSPAN4* knockout efficiency, a knock-in plasmid was constructed to insert mCherry into the chick *TSPAN4* gene under

control of the original promoter. mCherry was inserted into *TSPAN4* at the position targeted by the sgRNA. Thus, an mCherry-positive signal indicates that native *TSPAN4* gene expression was silenced simultaneously. Follow this targeting strategy (Extended Data Fig. 8a), the T4-Gallus-KO-mcherry-KI plasmid (PM19040-A) was constructed by Biocytogen, the detail design primer information is presented in Supplementary Table 1. The integration detection primers were as follows: PM19040-A-WT-F, 5'-GGTCCAGCACTGATGAGTCCACCTA-3'; PM19040-A-Mut-R, 5'-GGGGAAAGGACAGCTTCAGTAGTCG-3'; PM19040-A-WT-F, 5'-GGTCCAGCACTGATGAGTCCACCTA-3'; PM19040-A-WT-R, 5'-ACCATCTTGCCCAACTTCGAGTTCA-3'.

To generate the *TSPAN4*-KO chick embryos, a square hole ($0.6\text{ cm} \times 0.6\text{ cm}$) was cut in the eggshell of gastrulating chick embryos. A total of $1.2\text{ }\mu\text{g}$ of the gRNAs (target sequences are listed in STARMETHODS) were co-injected with $1\text{ }\mu\text{g}$ Cas9 and $1.6\text{ }\mu\text{g}$ mCherry-KI plasmid into chick embryos at Hamburger Hamilton stage 4 (embryonic 18 h) using a glass capillary with a tip diameter of 0.1 mm . Chick embryos were then electroporated using previously described techniques⁴⁶. The hole was covered by Parafilm, and the chick embryos were incubated at $37.5\text{ }^\circ\text{C}$ in the air under 70% humidity. Knockouts were confirmed by direct FACS for mCherry-positive signal sorting and by *in vivo* imaging for mCherry-positive signal detection.

Chick CAM angiogenesis assay

Fertilized chicken eggs were incubated at $37.5\text{ }^\circ\text{C}$ for 9 days and then opened so that the CAM could be observed. For preparation of Matrigel- or agarose-embedded migrasomes, first, $30\text{ }\mu\text{g}$ of purified migrasomes (from CAM of chicken embryos at E9d) were re-suspended in $3\text{ }\mu\text{l }1\times\text{ PBS}$. Second, the resuspended migrasomes were mixed with either $5\text{ }\mu\text{l}$ Matrigel (356234, BD) or 2% low-melting-point agarose. As the control, $3\text{ }\mu\text{l }1\times\text{ PBS}$ was mixed with $5\text{ }\mu\text{l}$ Matrigel or 2% low-melting-point agarose. Last, the congealed mixture was placed on the designated side of the CAM *in vivo*. In the following days, numerous allantoic vessels developed in a ‘spoked-wheel’ pattern. The newly formed vessels were examined and visualized with a photo microscope (Leica EZ4W). The density or number of newly formed capillaries in the CAM was quantified with ImageJ v1.8.0.112 or Image-Pro Plus software (Media Cybernetics).

CAM nylon mesh assay

The CAM nylon mesh assay was performed on fertilized SPF eggs (variety, White Leghorn; cleanliness, SPF) at 8–15 days of embryonic development. The nylon meshes (TS207-050, SK, pore size $300\text{ }\mu\text{m}$, China) were cut into 4.41 mm^2 pieces, then autoclaved for 10 min and vacuum-dried. Ten microlitres Matrigel and $5\text{ }\mu\text{l}$ collagen I mixed either with $5\text{ }\mu\text{l }1\times\text{ PBS}$ or with $5\text{ }\mu\text{l}$ migrasomes ($10\text{ }\mu\text{g }\mu\text{l}^{-1}$) were placed onto the nylon mesh and incubated at $37\text{ }^\circ\text{C}$ for 30 min and at $4\text{ }^\circ\text{C}$ for 1 h for polymerization. Polymerized meshes were placed onto the outer region of CAM8d and incubated. To visualize vessels, $20\text{ }\mu\text{l}$ of dextran-fluorescein isothiocyanate (FITC) ($2\text{ }\mu\text{g }\mu\text{l}^{-1}$, Sigma) was injected into the chick bloodstream. After 15 min of incubation, the newly formed vessels were examined and visualized with a photo microscope (Leica EZ4W) or by Andor spinning disk microscopy. The density or number of newly formed capillaries in the CAM was quantified with ImageJ v1.8.0.112 or Image-Pro Plus software (Media Cybernetics).

CAM ex vivo sprouting assay

A total of $150\text{ }\mu\text{l}$ Matrigel and $30\text{ }\mu\text{l}$ collagen I were mixed on ice, and then this matrix mixture was added into 3.5 mm confocal dishes and incubated at $37\text{ }^\circ\text{C}$ for 1 h for polymerization. Next, dissected CAMs (about 1 mm^2) from E8d were collected and embedded in the matrix. After 24 h, drops of soft agarose with or without migrasomes were added on opposite sides of the CAM. After another 5 days of culture, ECs sprouting from CAMs were visualized by Nikon Ti2-E and analysed by Nikon NIS-elements. To assess the role of migrasomes in

chemo-attraction of ECs and tip cell filopodia formation, post-treated CAMs were stained by ASM1 and actin, then the samples were visualized by Nikon A1 confocal microscopy.

Factor detection in migrosome of mouse BMM

Mouse bone marrow monocytes (BMMs) were acquired from WT C57BL/6 mice using the EasySep mouse monocyte isolation kit. Briefly, bone marrow cell suspensions ($1 \times 10^8\text{ cells ml}^{-1}$) were incubated sequentially with isolation cocktail component and Dextran Rapid Spheres. Unwanted cells (T cells, B cells, natural killer cells, dendritic cells and so on) were labelled with antibodies combined with magnetic particles, and separated from unlabelled cells (monocytes) by a magnet. For purity assessment, cells stained with CD115 and Ly6C antibodies were analysed by flow cytometry. BMMs were grown in RPMI 1640 (C11875500BT, Gibco) supplemented with 10% FBS, 2 mM GlutaMAX and 100 U ml^{-1} penicillin/streptomycin in 5 CO_2 at $37\text{ }^\circ\text{C}$. BMMs were activated with 20 ng ml^{-1} M-CSF for 12–24 h, then fixed by 4% paraformaldehyde and stained by WGA or antibodies against CD115, VEGFA or CXCL12. Then the samples were visualized by Nikon A1 confocal.

Single-cell RNA-seq and data analysis

WGA^{high} CAM cells were sorted by FACS into PCR tubes. Single-cell RNA-seq experiments were performed according to the Smart-seq2 protocol with 20 cDNA pre-amplification cycles. Samples were sequenced by Illumina HiSeq 4000 with 150 bp paired-end reads. The transcriptome was quantified by Salmon with the chicken genome reference GRCg6a. Data from cells with more than 1,500 genes detected were considered as high quality and were used for subsequent analysis. Further data analysis and visualization used Seurat.

Identification of monocyte-like cells

Annotated homologues of many classical cell-type marker genes could not be found in the chicken reference genome. Therefore, we collected all reported classical and non-classical marker genes for the cell types we suspected on the basis of morphology data. The collection of classical and non-classical marker genes contained experimental results and single-cell RNA-seq results from <http://biocc.hrbmu.edu.cn/CellMarker/>. In total, 317 high-expression genes were found in the monocyte-like cell group (Fig. 2g).

Statistics and reproducibility

All statistical analyses were performed using GraphPad Prism7 software. No data were excluded from the analyses. No statistical method was used to pre-determine sample size. Samples and images related in all experiments were acquired randomly. The investigators were not blinded to allocation during experiments and outcome assessment. Data are expressed as mean \pm standard error of the mean (s.e.m.) from at least three separate experiments performed in triplicate. Comparisons in Figs. 6i and 7c,e and Extended Data Fig. 6b, were performed by using one-way analysis of variance (ANOVA) unpaired multiple comparisons. Comparisons in Extended Data Figs. 5b, 7f and 9e were performed by using two-way ANOVA unpaired multiple comparisons. Comparisons in all other figures were performed by two-tailed, unpaired Student's *t*-tests. A value of $P < 0.05$ was considered statistically significant. A description of each statistical test and the *n* and *P* values are included with each legend or experimental source data. The number of experimental repeats are specified in the figure legends. The experiments in Figs. 1a,b,d,f-i, 2e,j,k, 3a, 4b,c and 5q and Extended Data Figs. 8b and 9c were conducted three times independently with similar results. The experiments in Fig. 4h,i,j were conducted twice independently with similar results. The experiments in Figs. 5a and 6k and Extended Data Fig. 4a,b were conducted four times independently with similar results. All other experiments were performed at least three independent times with similar results unless specified in the legends.

Reporting summary

Further information on research design is available in the Nature Portfolio Reporting Summary linked to this article.

Data availability

RNA-seq data that support the findings of this study have been deposited in the National Center for Biotechnology Information Sequence Read Archive under the accession code SAMN30722995. The mass spectrometry proteomics data have been deposited in ProteomeXchange Consortium via the PRIDE partner repository with the dataset identifier or the primary accession code [PXD036647](#). The statistical source data for all figures and extended data figures have been provided as numerical source data. All other data supporting the findings of this study are available from the corresponding author on reasonable request. Further information and requests for resources and reagents should be directed to and will be fulfilled by L.Y. Source data are provided with this paper.

References

46. Sauka-Spengler, T. & Barembaum, M. Gain- and loss-of-function approaches in the chick embryo. *Methods Cell. Biol.* **87**, 237–256 (2008).

Acknowledgements

We are grateful to the members of the Yu groups for their helpful discussions and suggestions. This research was supported by the Ministry of Science and Technology of the People's Republic of China (grant no. 2017YFA0503404), the National Natural Science Foundation of China (grant nos. 31790401, 92054301 and 32030023) and the Beijing Municipal Science & Technology Commission (grant nos. Z201100005320019 and Z211100003321002) and internal grant from Tsinghua university (2030 plan). We thank the State Key Laboratory of Membrane Biology for facility support and assistance with spinning disk microscopy. We thank the Protein Chemistry Facility at the Centre for Biomedical Analysis of Tsinghua University for mass spectrometry sample analysis. We acknowledge the assistance of the Imaging Core Facility, Technology Center for Protein Sciences, Tsinghua University for assistance with Imaris analysis. We acknowledge the assistance of

SLSTU-Nikon Biological Imaging Center for assistance with using the NIKON A1RSiHD25 laser scanning confocal microscope and software. We thank the Core Facility, Center of Biomedical Analysis, Tsinghua University for technical support with flow cytometry and data analysis.

Author contributions

L.Y. conceived the project. L.Y. and C.Z. designed and C.Z. performed in vitro and in vivo experiments and analysed data. L.Y. and C.Z. wrote the manuscript. M.G., Y.L. and M.S. performed migrasome 3D reconstruction experiments. S.Y. and H.H. performed *TSPAN4*-KO and monocyte depletion experiments. T.L. and J.W. designed and performed the single-cell sequencing experiment. D.J. performed migrasome purification experiments. All authors discussed the manuscript, commented on the project and contributed to the preparation of the paper.

Competing interests

L.Y. is the scientific founder of Migrasome therapeutics Ltd. All other authors declare no conflicts of interest.

Additional information

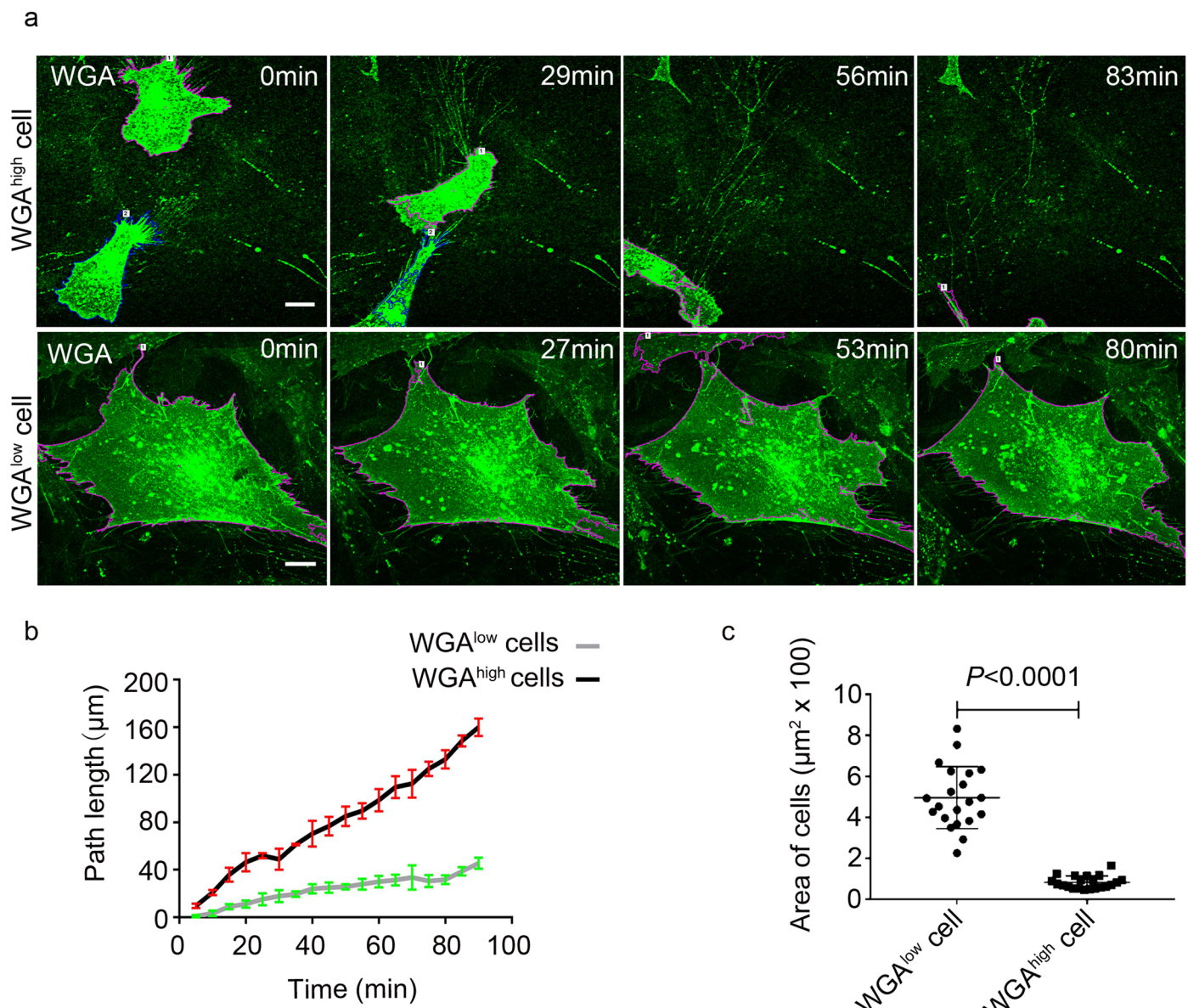
Extended data is available for this paper at
<https://doi.org/10.1038/s41556-022-01026-3>.

Supplementary information The online version contains supplementary material available at
<https://doi.org/10.1038/s41556-022-01026-3>.

Correspondence and requests for materials should be addressed to Li Yu.

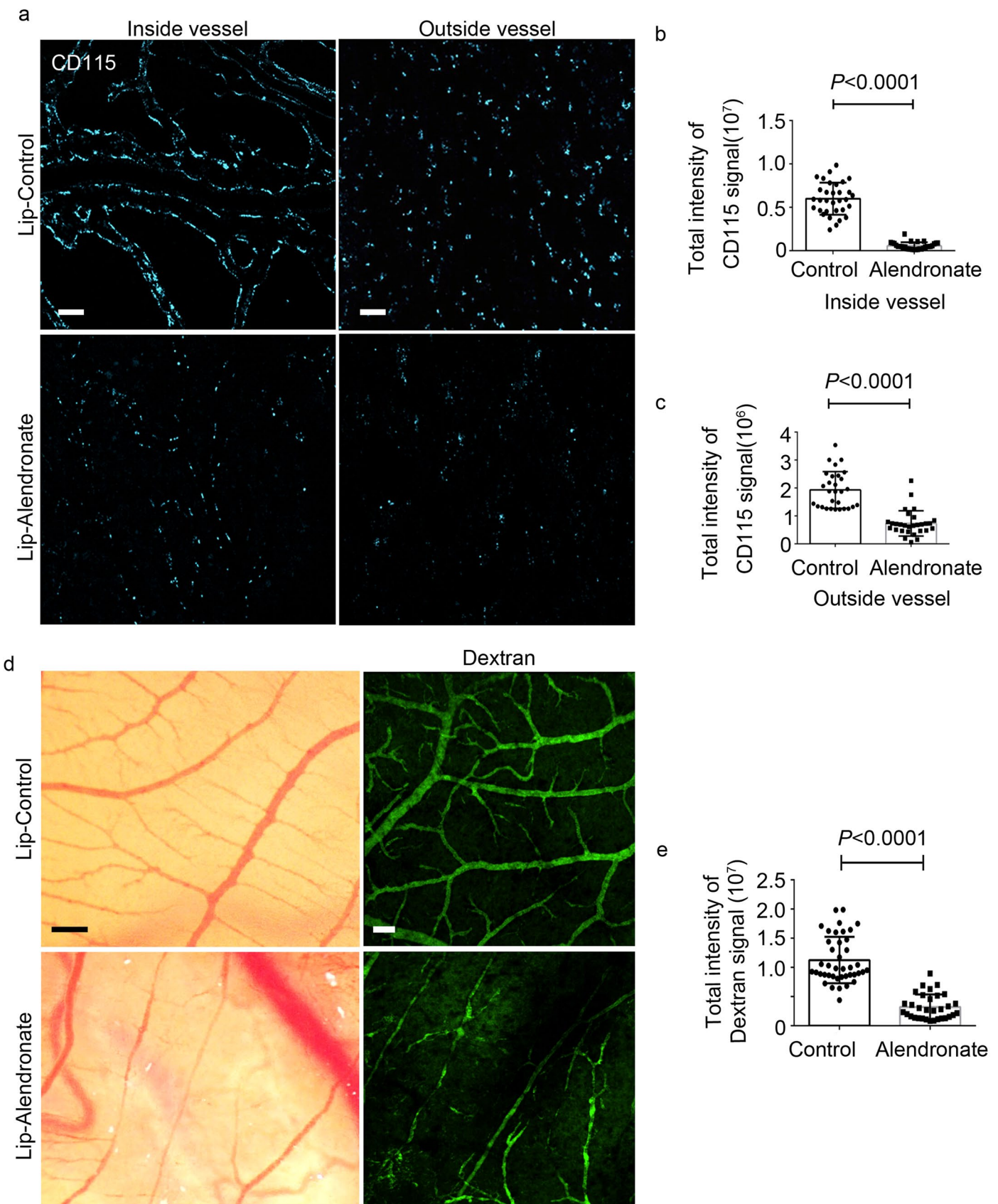
Peer review information *Nature Cell Biology* thanks Rajendra Apte, Michael Sixt and the other, anonymous, reviewer(s) for their contribution to the peer review of this work.

Reprints and permissions information is available at
www.nature.com/reprints.



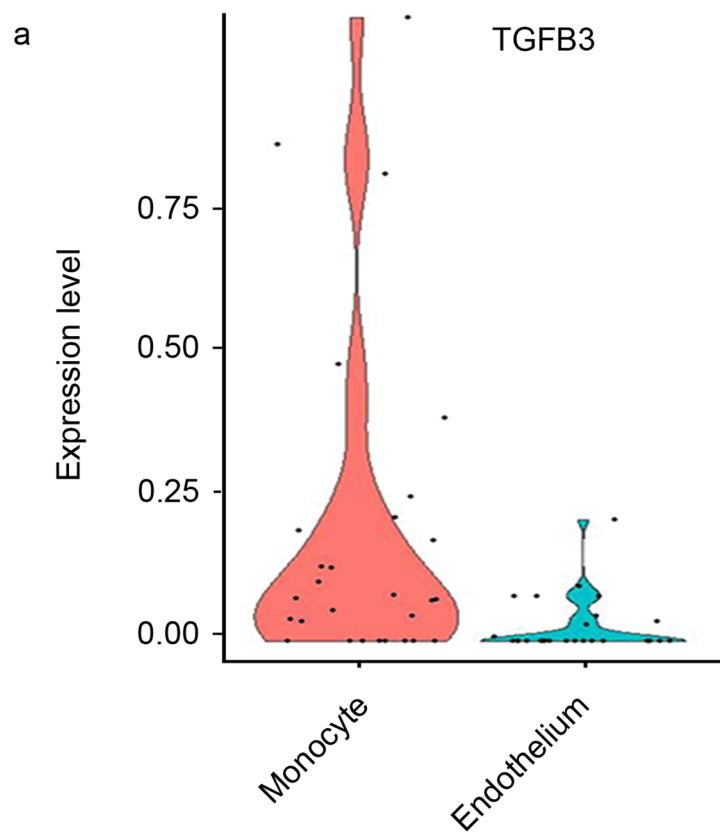
Extended Data Fig. 1 | Morphology of WGA^{high/low} cell. (a) Migration of WGA^{high} and WGA^{low} cells was monitored by time-lapse confocal microscopy. Scale bar, 5 μm . (b) Cells from (a) were quantified for migration speed. Data are presented as means \pm SEM; n = 21 cells per group pooled from three independent experiments.

(c) Cells from (a) were quantified for size. Data are presented as means \pm SEM; n = 21 cells per group pooled from three independent experiments. P values were calculated using a two-tailed, unpaired t-test, $P < 0.0001$. Source numerical data are available in source data.



Extended Data Fig. 2 | See next page for caption.

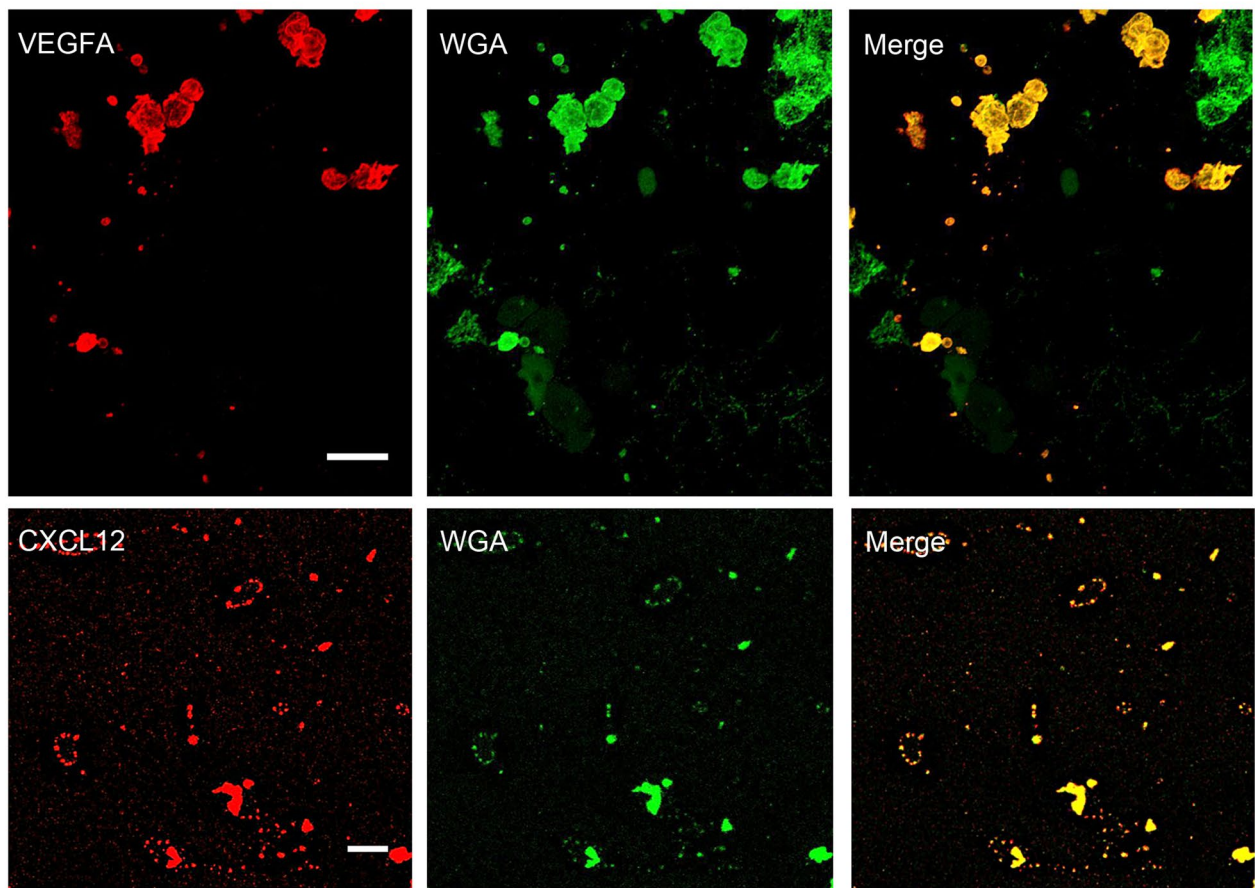
Extended Data Fig. 2 | Monocytes depletion by alendronate impairs angiogenesis. (a) After treatment with control liposomes or alendronate liposomes, CAM9d were stained by CD115-Alexa488 to detect monocytes inside and outside the blood vessels. Inside vessels: CD115-Alexa488 was microinjected into the CAM vasculature. Outside vessels: CD115-Alexa488 was add onto the CAM surface. Images were taken 30 minutes after CD115-Alexa488 staining. Scale bar, 50 μ m. (b-c) The numbers of monocytes inside or outside vessels were quantified according to the CD115 signal. Data are presented as mean \pm SEM; n = 32 samples from three independent experiments; P values were calculated using a two-tailed, unpaired t-test, P < 0.0001. (d) CAMs treated with control liposomes and alendronate liposomes were visualized with a stereomicroscope (left panel) or a confocal microscope after dextran-FITC microinjection (right panel). Scale bar, left panel, 500 μ m; right panel, 50 μ m. (e) The number of sprouting capillaries from (d) was quantified according to the intensity of the dextran signal. Data are presented as mean \pm SEM; n = 32 samples from three independent experiments; P values were calculated using a two-tailed, unpaired t-test, P < 0.0001. Source numerical data are available in source data.



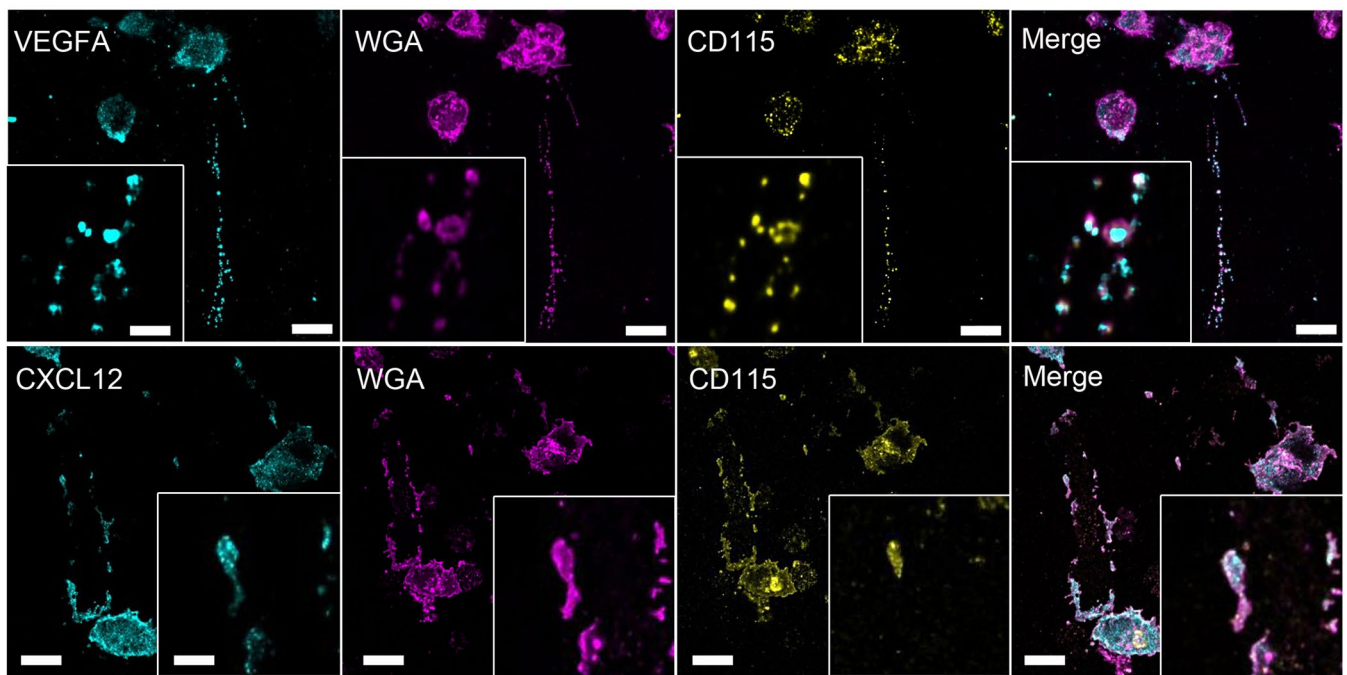
Extended Data Fig. 3 | mRNA levels of *TGFB3* by single-cell sequencing. (a) Violin plots showing the mRNA levels of *TGFB3* from single-cell sequencing analysis of monocyte and endothelium cells.

a

CAM9d



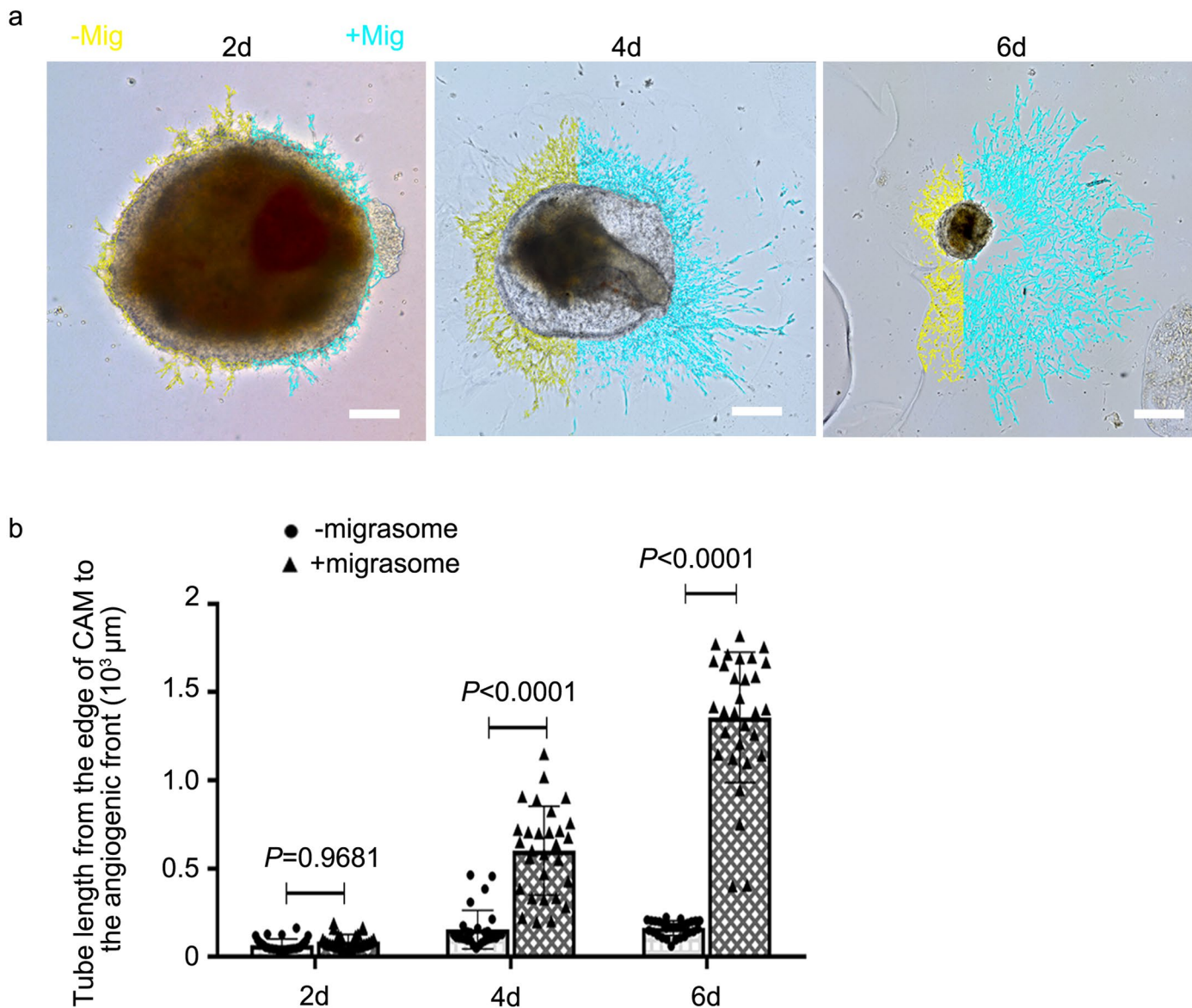
b



Extended Data Fig. 4 | See next page for caption.

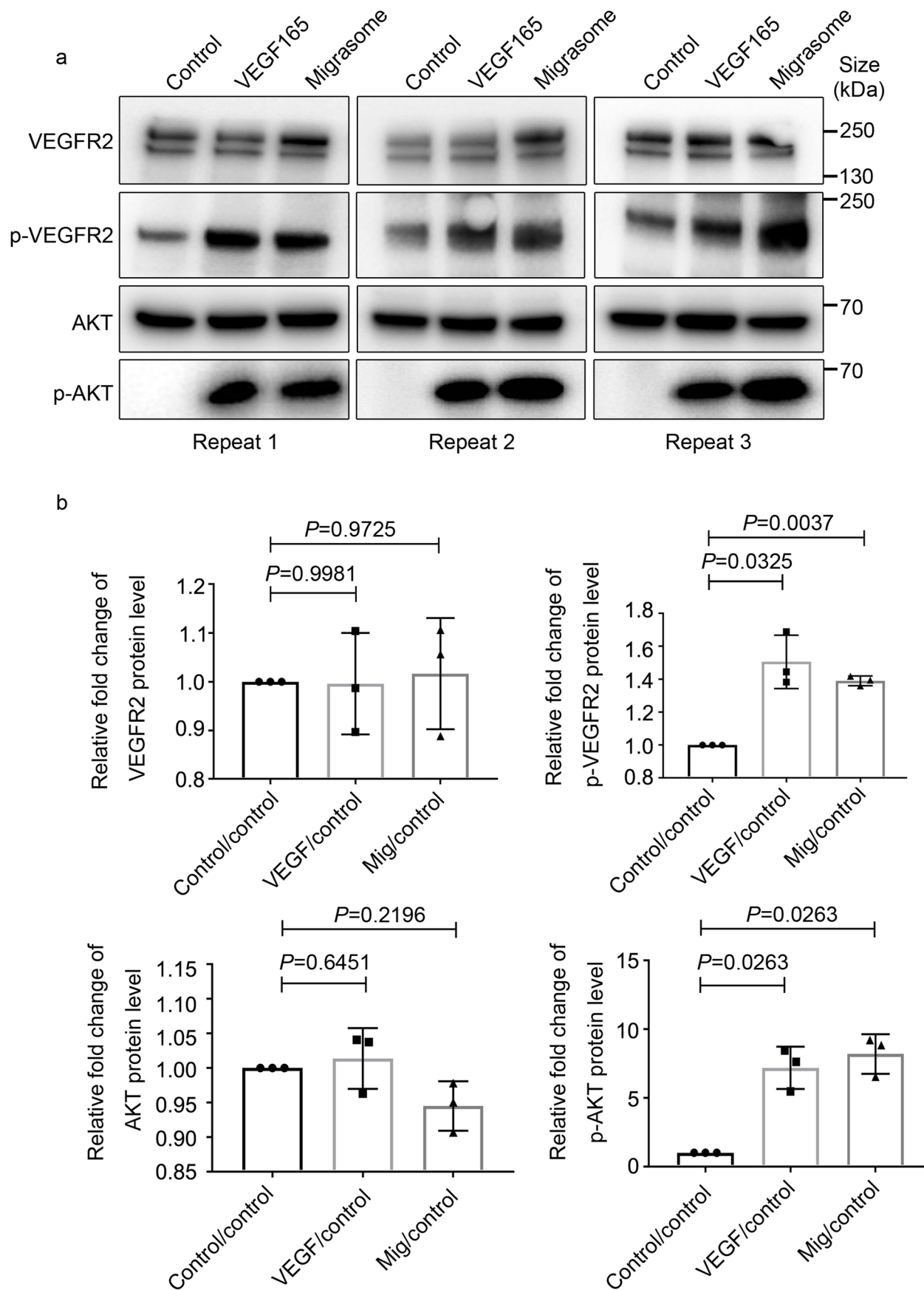
Extended Data Fig. 4 | VEGFA/CXCL12 are enriched in migrasomes from CAM or mouse monocytes. (a) CAM9d were stained with WGA and the indicated antibodies and visualized by confocal microscopy. Scale bar, 20 μm . Immunofluorescence in CAMs was visualized by confocal z-stack imaging and presented as the maximum intensity projection. (b) Migrasomes from

mouse monocytes are enriched with VEGFA and CXCL12. Mouse bone marrow monocytes (BMMs) acquired from WT C57BL/6 mice were stained with WGA and the indicated antibodies and visualized by confocal microscopy. Scale bar, 10 μm . Enlarged images of migrasomes are shown in the white boxes. Scale bar, 2.5 μm .



Extended Data Fig. 5 | Migrasome delivery promotes EC proliferation and sprouting. (a) Dissected CAMs from E8d were mounted on the top of a collagen I-Matrigel matrix mix, and soft agarose with migrasomes (+Mig) or without migrasomes (-Mig) was added on opposite sides of the CAM. 2, 4 and 6 days after mounting, the samples were visualized by confocal microscopy. Scale bar, 200 μm . (b) The proliferation of ECs and sprouting progression from (a) was

quantified by the tube length from the edge of CAM to the angiogenic front. Data are presented as mean \pm SEM; $n=30$ fields of CAM leaflets from five independent experiments; P values were calculated using a two-way ANOVA unpaired multiple comparisons, N.S: no significance ($P=0.9681$); $P < 0.0001$. Source numerical data are available in source data.

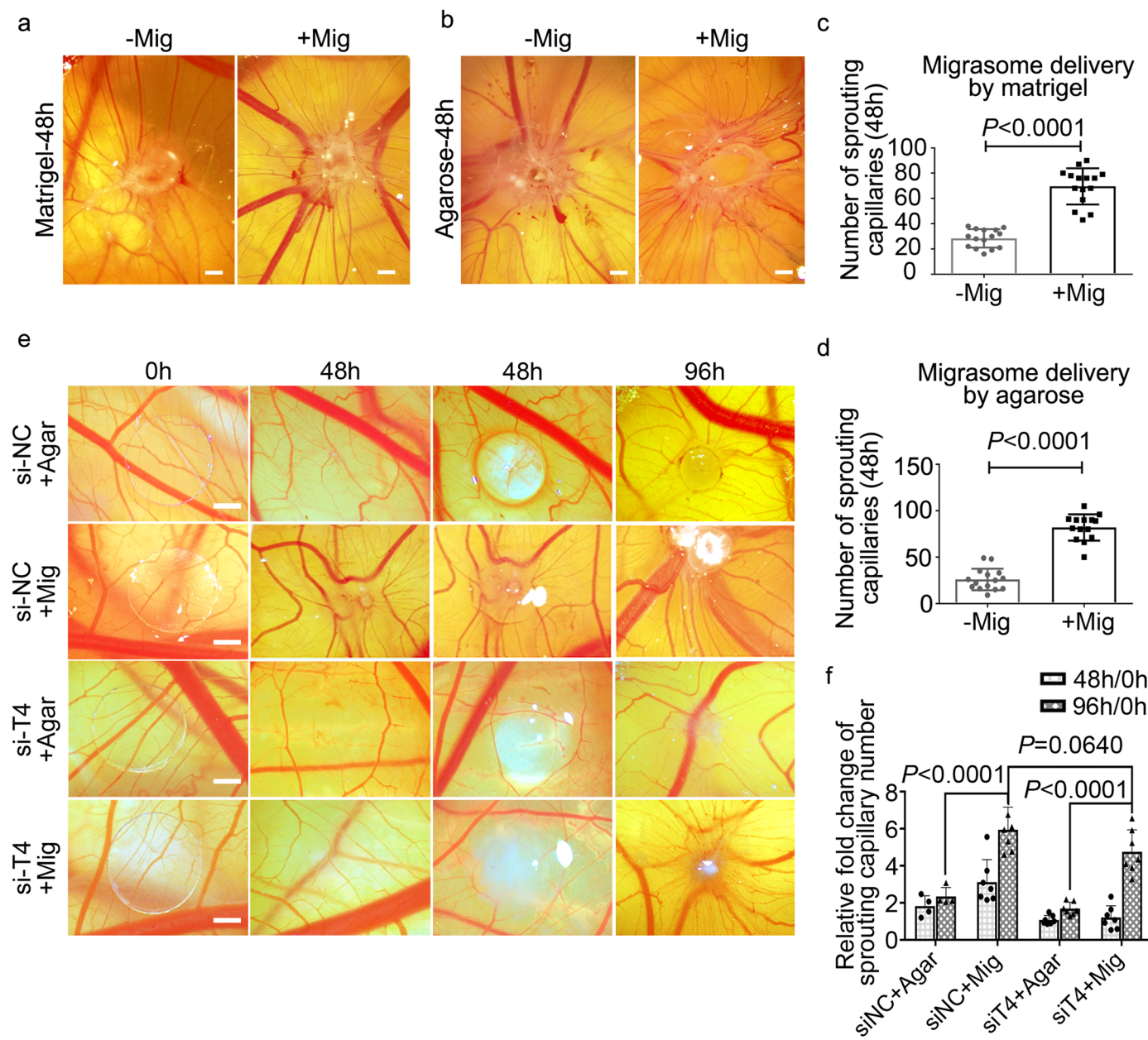


Extended Data Fig. 6 | See next page for caption.

Extended Data Fig. 6 | Migrasome triggers VEGFR2 and AKT phosphorylation.

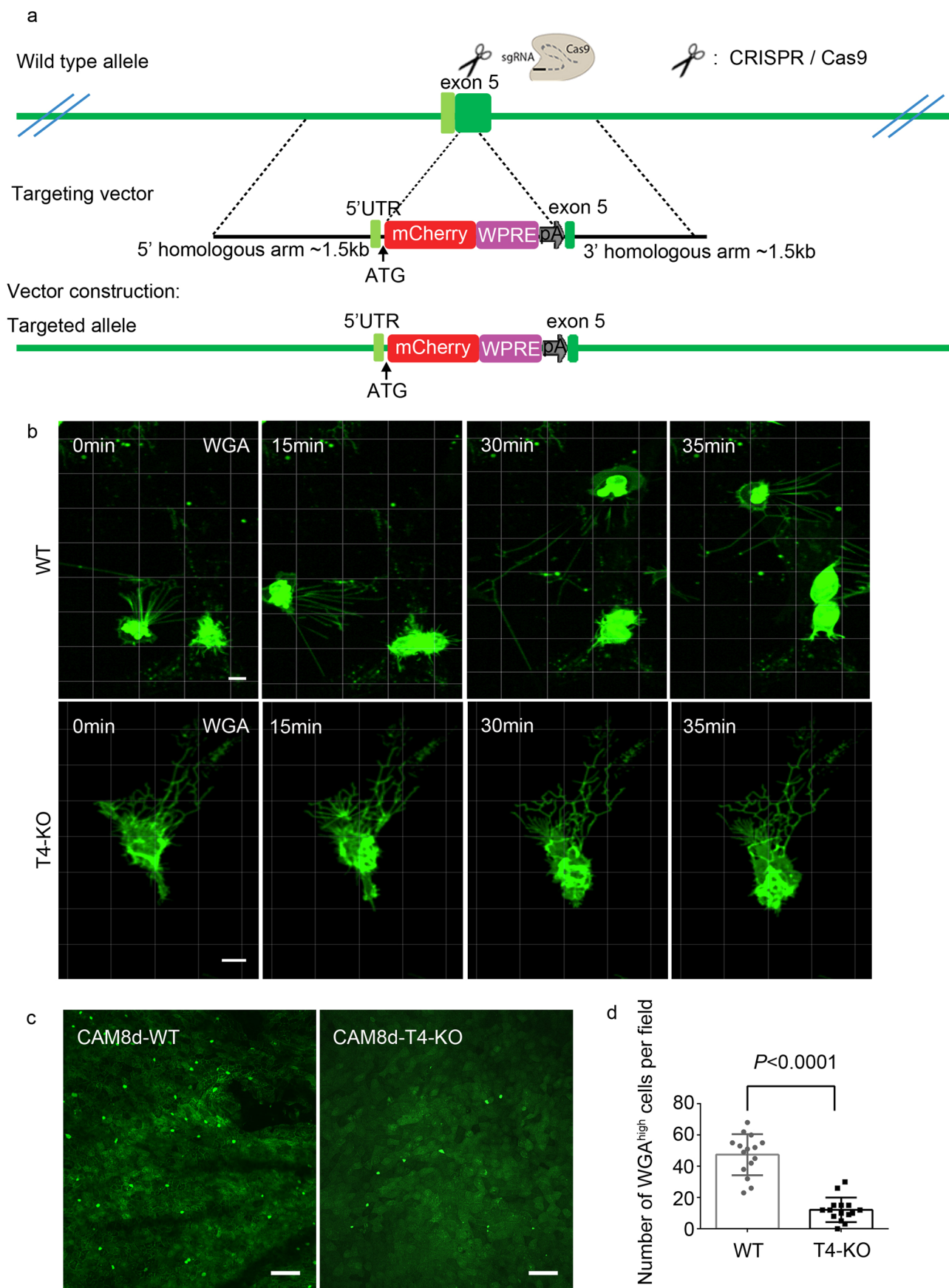
(a) Cells were treated with migrasome or VEGF165 for 24 hours and the Lysates of cell were analysed by western blot using indicated antibody. 3 repeats were shown (repeat 1 is figure 5q). **(b)** The relative fold change of indicated signal in the control, VEGF165 and migrasome treated cells was quantified. Data are presented as mean \pm SEM; n = 3 from three independent experiments; P values were calculated using a one-way ANOVA unpaired multiple comparisons. VEGFR2 protein level: (N.S: no significance; P=0.9981,

Control/control vs. VEGF/control; P=0.9725, Control/control vs. Mig/control). p-VEGFR2 protein level: (P=0.0325, Control/control vs. VEGF/control; P=0.0037, Control/control vs. Mig/control). AKT protein level: (N.S: no significance; P=0.6451, Control/control vs. VEGF/control; P=0.2196, Control/control vs. Mig/control). p-AKT protein level: (P=0.0263, Control/control vs. VEGF/control; P=0.0263, Control/control vs. Mig/control). Source numerical data and unprocessed blots are available in source data.



Extended Data Fig. 7 | Migrasomes rescue TSPAN4 KD induced capillarization and monocyte recruitment defects. (a) Migrasomes were delivered to CAM9d by mixing them with Matrigel. After 48 h, CAMs were visualized by stereomicroscopy. Scale bar, 500 μ m. (b) Migrasomes were delivered to CAM9d by mixing them with low-melting-point agarose. After 48 h, CAMs were visualized by stereomicroscopy. Scale bar, 500 μ m. (c) CAMs from (a) were quantified for the number of newly formed capillaries. Data are presented as mean \pm SEM; n = 15 fields from three independent experiments; P values were calculated using a two-tailed, unpaired t-test, P < 0.0001. (d) CAMs from (b) were quantified for the number of sprouting capillaries. Data are presented as mean \pm SEM; n = 15

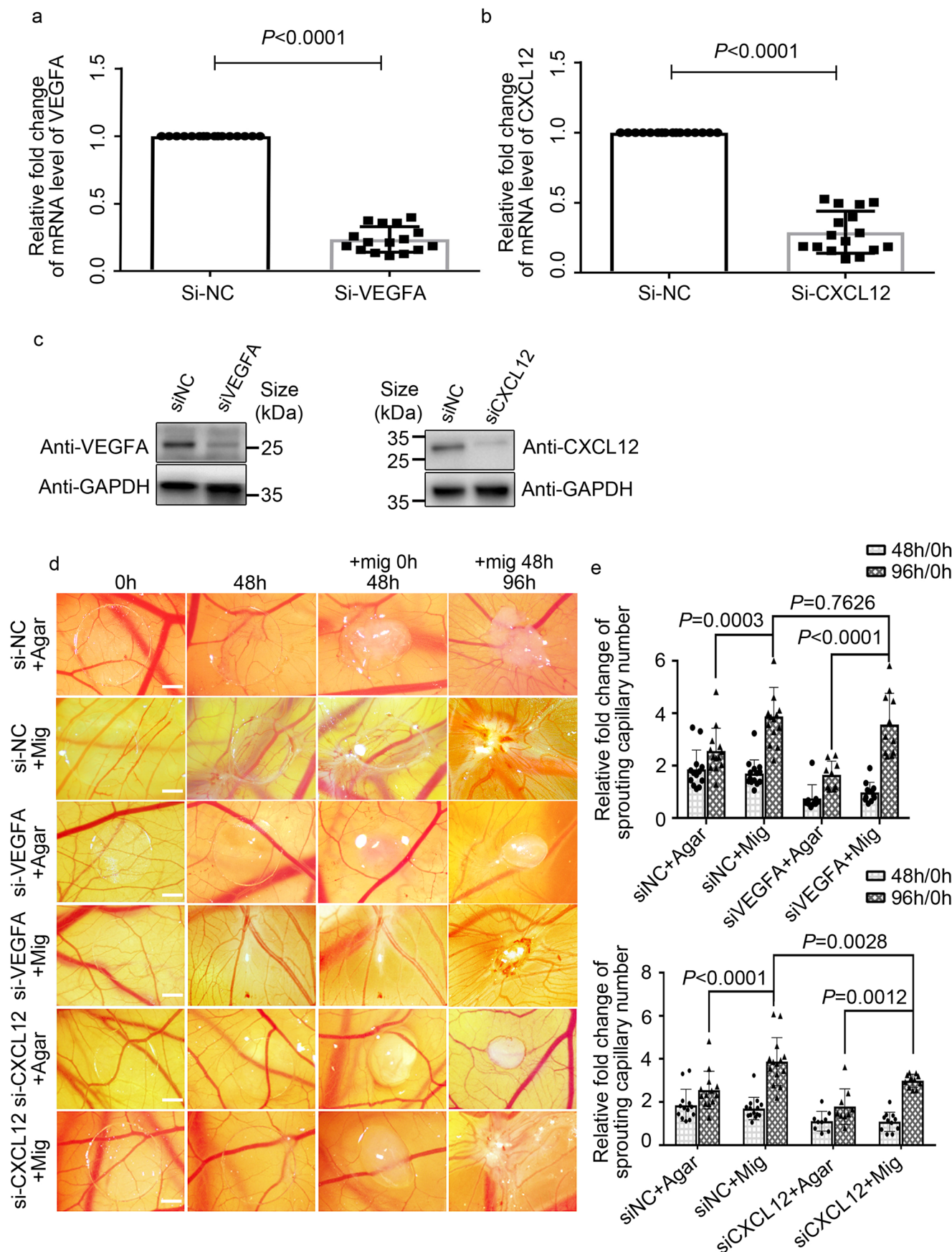
fields from three independent experiments; P values were calculated using a two-tailed, unpaired t-test, P < 0.0001. (e) 48 h after transfection with control of TSPAN4 (T4) siRNA, migrasomes embedded in low-melting-point agarose were added to CAMs. 48 h later, CAMs were visualized by stereomicroscopy. Scale bar, 500 μ m. (f) CAMs from (e) were quantified for the relative change in the number of sprouting capillaries. Data are presented as means \pm SEM, n = 7 fields from three independent experiments, P values were calculated using a two way ANOVA unpaired multiple comparisons, N.S: no significance (P=0.0640), P < 0.0001. Source numerical data are available in source data.



Extended Data Fig. 8 | See next page for caption.

Extended Data Fig. 8 | *TSPAN4* KO impairs migrasome formation. **(a)** Diagram showing the strategy for knocking out *TSPAN4* and knocking in mCherry in chick embryos. The mCherry coding sequence was inserted into *TSPAN4* at the position targeted by the sgRNA. Thus, an mCherry-positive signal indicates that native *TSPAN4* gene expression was silenced simultaneously. **(b)** Time-lapse imaging of migration and migrasome formation by WGAhigh cells isolated from WT or *TSPAN4*-KO CAM8d. Cells were stained by WGA and observed by spinning disk

microscopy. Scale bar, 5 μm. **(c)** CAMs from Fig. 6k and 6l were stained for WGA and observed by spinning disk microscopy. Scale bar, 30 μm. **(d)** CAMs from Fig. 6k and 6l were quantified for the number of WGAhigh cells. Data are presented as mean ± SEM; n = 15 cells from three independent experiments; P values were calculated using a two-tailed, unpaired t-test, P < 0.0001. Source numerical data are available in source data.



Extended Data Fig. 9 | See next page for caption.

Extended Data Fig. 9 | Migrasomes rescue VEGFA/CXCL12 KD induced capillarization and monocyte recruitment defects. (a) CAMs were treated with VEGFA siRNA. 72 h after transfection, the CAMs were harvested, and the VEGFA knockdown efficiency in the CAMs was determined using q-PCR. Data are presented as mean \pm SEM; n = 16 pieces from three independent experiments; P values were calculated using a two-tailed, unpaired t-test, P < 0.0001. (b) CAMs treated with CXCL12 siRNA for 72 h were harvested, and CXCL12 knockdown efficiency in CAM pieces was detected by q-PCR. Data are presented as mean \pm SEM; n = 16 pieces from three independent experiments; P values were calculated using a two-tailed, unpaired t-test, P < 0.0001. (c) VEGFA and CXCL12 knockdown efficiencies in siRNA-treated CAM pieces were determined by western blot analysis using then indicated antibodies. (d) CAMs were transfected with the indicated siRNAs. After 48 h, migrasomes embedded in

low-melting-point agarose were added. After another 48 h, CAMs were visualized by stereomicroscopy. Scale bar, 1 mm. (e) CAMs treated with VEGF siRNA (top) or CXCL12 siRNA (bottom) from (d) were quantified for the change in the number of sprouting capillaries. Data are presented as mean \pm SEM; n = 9 fields from three independent experiments; in siVEGFA group, P values were calculated using a two way ANOVA unpaired multiple comparisons, N.S: no significance (P=0.7626, 96h/0h, siNC+Migrasome vs. siVEGFA+Migrasome); P = 0.0003(96h/0h, siNC+Agarose vs. siNC+Migrasome); P < 0.0001; in siCXCL12 group, P values were calculated using a two way ANOVA unpaired multiple comparisons, P=0.0028 (96h/0h, siNC+Migrasome vs. siCXCL12+Migrasome); P=0.0012 (96h/0h, siCXCL12+Agarose vs. siCXCL12+Migrasome); P<0.0001. Source numerical data and unprocessed blots are available in source data.

Corresponding author(s): Li Yu

Last updated by author(s): Sep 30, 2022

Reporting Summary

Nature Portfolio wishes to improve the reproducibility of the work that we publish. This form provides structure for consistency and transparency in reporting. For further information on Nature Portfolio policies, see our [Editorial Policies](#) and the [Editorial Policy Checklist](#).

Statistics

For all statistical analyses, confirm that the following items are present in the figure legend, table legend, main text, or Methods section.

n/a Confirmed

- The exact sample size (n) for each experimental group/condition, given as a discrete number and unit of measurement
- A statement on whether measurements were taken from distinct samples or whether the same sample was measured repeatedly
- The statistical test(s) used AND whether they are one- or two-sided
Only common tests should be described solely by name; describe more complex techniques in the Methods section.
- A description of all covariates tested
- A description of any assumptions or corrections, such as tests of normality and adjustment for multiple comparisons
- A full description of the statistical parameters including central tendency (e.g. means) or other basic estimates (e.g. regression coefficient) AND variation (e.g. standard deviation) or associated estimates of uncertainty (e.g. confidence intervals)
- For null hypothesis testing, the test statistic (e.g. F , t , r) with confidence intervals, effect sizes, degrees of freedom and P value noted
Give P values as exact values whenever suitable.
- For Bayesian analysis, information on the choice of priors and Markov chain Monte Carlo settings
- For hierarchical and complex designs, identification of the appropriate level for tests and full reporting of outcomes
- Estimates of effect sizes (e.g. Cohen's d , Pearson's r), indicating how they were calculated

Our web collection on [statistics for biologists](#) contains articles on many of the points above.

Software and code

Policy information about [availability of computer code](#)

Data collection	Images are acquired by FV31S-SW V2.3.1 (Olympus), ZEN 2014 (Zeiss), Velocity 6.3.1 (PerkinElmer), andor spinning disk confocal dragonfly200 (Andor technology Ltd, Belfast , UK), Nikon A1 confocal (HD25RSi LSCM). Flow cytometry data was acquired by MoFlo Astrios EQ or MoFlo XDP (beckMan).
Data analysis	Imaris v8.1.4 & 9.5.0 were used for analysis of cell tracker, cell migrating speed and migrasomes chemoattractant movie processing. Amira 6.0.0 software was used for surface processing of CAM images. NIS-Element AR analysis was used for cell tracking. Image J v1.8.0.112 was used for analysis of number of sprouting capillary, number of cell, vesicles diameter, relative intensity and migrasomes accumulation images. CytoFLEX S or CytoFLEX LX was use for flow cytometry data analysis. Proteome Discoverer 2.3 were used for mass spectrum data analysis. GraphPad Prism 7 was used for statistic analysis.

For manuscripts utilizing custom algorithms or software that are central to the research but not yet described in published literature, software must be made available to editors and reviewers. We strongly encourage code deposition in a community repository (e.g. GitHub). See the Nature Portfolio [guidelines for submitting code & software](#) for further information.

Data

Policy information about [availability of data](#)

All manuscripts must include a [data availability statement](#). This statement should provide the following information, where applicable:

- Accession codes, unique identifiers, or web links for publicly available datasets
- A description of any restrictions on data availability
- For clinical datasets or third party data, please ensure that the statement adheres to our [policy](#)

RNA sequencing data that support the findings of this study have been deposited in the National Center for Biotechnology Information Sequence Read Archive under the accession codes SAMN30722995. The mass spectrometry proteomics data have been deposited in ProteomeXchange Consortium via the PRIDE partner repository with the dataset identifier or the primary accession code PXD036647. The statistical source data for all Figs. and Extended data Figs. have been provided as "Numerical Source Data". All other data supporting the findings of this study are available from the corresponding author on reasonable request. Further information and requests for resources and reagents should be directed to and will be fulfilled by Li Yu.

Human research participants

Policy information about [studies involving human research participants and Sex and Gender in Research](#).

Reporting on sex and gender This study did not involve human research partipants

Population characteristics This study did not involve human research partipants

Recruitment This study did not involve human research partipants

Ethics oversight This study did not involve human research partipants

Note that full information on the approval of the study protocol must also be provided in the manuscript.

Field-specific reporting

Please select the one below that is the best fit for your research. If you are not sure, read the appropriate sections before making your selection.

Life sciences Behavioural & social sciences Ecological, evolutionary & environmental sciences

For a reference copy of the document with all sections, see nature.com/documents/nr-reporting-summary-flat.pdf

Life sciences study design

All studies must disclose on these points even when the disclosure is negative.

Sample size No statistical methods were used to determine sample size. For all the experiments, we followed the routine practice in the similar studying fields. And it has been our routine practice to conduct experiments upon a relatively large but reasonable size.

Data exclusions No data were excluded from the analysis.

Replication Attempts at replication were successful. For all experiments, except experiments related to Figs. 4h, 4i, 4j, were conducted twice independently with similar results., at least 3 times independent experiments were repeated with the similar results as presented in this study. Detail information was involved in the Methods---Statistics and reproducibility section, as well as Statistics Source Data.

Randomization Samples and images related in all experiments were acquired randomly.

Blinding The investigators were not blinded to allocation during experiments and outcome assessment. Within each experiment, at least one negative control group was set to ensure that only one variate was tested. And because all the data were conducted based on random sampling and reasonably large sample size, blinding is not relevant to this study.

Behavioural & social sciences study design

All studies must disclose on these points even when the disclosure is negative.

Study description Briefly describe the study type including whether data are quantitative, qualitative, or mixed-methods (e.g. qualitative cross-sectional, quantitative experimental, mixed-methods case study).

Research sample

State the research sample (e.g. Harvard university undergraduates, villagers in rural India) and provide relevant demographic information (e.g. age, sex) and indicate whether the sample is representative. Provide a rationale for the study sample chosen. For studies involving existing datasets, please describe the dataset and source.

Sampling strategy

Describe the sampling procedure (e.g. random, snowball, stratified, convenience). Describe the statistical methods that were used to predetermine sample size OR if no sample-size calculation was performed, describe how sample sizes were chosen and provide a rationale for why these sample sizes are sufficient. For qualitative data, please indicate whether data saturation was considered, and what criteria were used to decide that no further sampling was needed.

Data collection

Provide details about the data collection procedure, including the instruments or devices used to record the data (e.g. pen and paper, computer, eye tracker, video or audio equipment) whether anyone was present besides the participant(s) and the researcher, and whether the researcher was blind to experimental condition and/or the study hypothesis during data collection.

Timing

Indicate the start and stop dates of data collection. If there is a gap between collection periods, state the dates for each sample cohort.

Data exclusions

If no data were excluded from the analyses, state so OR if data were excluded, provide the exact number of exclusions and the rationale behind them, indicating whether exclusion criteria were pre-established.

Non-participation

State how many participants dropped out/declined participation and the reason(s) given OR provide response rate OR state that no participants dropped out/declined participation.

Randomization

If participants were not allocated into experimental groups, state so OR describe how participants were allocated to groups, and if allocation was not random, describe how covariates were controlled.

Ecological, evolutionary & environmental sciences study design

All studies must disclose on these points even when the disclosure is negative.

Study description

Briefly describe the study. For quantitative data include treatment factors and interactions, design structure (e.g. factorial, nested, hierarchical), nature and number of experimental units and replicates.

Research sample

*Describe the research sample (e.g. a group of tagged *Passer domesticus*, all *Stenocereus thurberi* within Organ Pipe Cactus National Monument), and provide a rationale for the sample choice. When relevant, describe the organism taxa, source, sex, age range and any manipulations. State what population the sample is meant to represent when applicable. For studies involving existing datasets, describe the data and its source.*

Sampling strategy

Note the sampling procedure. Describe the statistical methods that were used to predetermine sample size OR if no sample-size calculation was performed, describe how sample sizes were chosen and provide a rationale for why these sample sizes are sufficient.

Data collection

Describe the data collection procedure, including who recorded the data and how.

Timing and spatial scale

Indicate the start and stop dates of data collection, noting the frequency and periodicity of sampling and providing a rationale for these choices. If there is a gap between collection periods, state the dates for each sample cohort. Specify the spatial scale from which the data are taken

Data exclusions

If no data were excluded from the analyses, state so OR if data were excluded, describe the exclusions and the rationale behind them, indicating whether exclusion criteria were pre-established.

Reproducibility

Describe the measures taken to verify the reproducibility of experimental findings. For each experiment, note whether any attempts to repeat the experiment failed OR state that all attempts to repeat the experiment were successful.

Randomization

Describe how samples/organisms/participants were allocated into groups. If allocation was not random, describe how covariates were controlled. If this is not relevant to your study, explain why.

Blinding

Describe the extent of blinding used during data acquisition and analysis. If blinding was not possible, describe why OR explain why blinding was not relevant to your study.

Did the study involve field work?

Yes No

Field work, collection and transport

Field conditions

Describe the study conditions for field work, providing relevant parameters (e.g. temperature, rainfall).

Location

State the location of the sampling or experiment, providing relevant parameters (e.g. latitude and longitude, elevation, water depth).

Access & import/export

Describe the efforts you have made to access habitats and to collect and import/export your samples in a responsible manner and in

Access & import/export

compliance with local, national and international laws, noting any permits that were obtained (give the name of the issuing authority, the date of issue, and any identifying information).

Disturbance

Describe any disturbance caused by the study and how it was minimized.

Reporting for specific materials, systems and methods

We require information from authors about some types of materials, experimental systems and methods used in many studies. Here, indicate whether each material, system or method listed is relevant to your study. If you are not sure if a list item applies to your research, read the appropriate section before selecting a response.

Materials & experimental systems

- | | |
|-----|--|
| n/a | <input type="checkbox"/> Involved in the study
<input checked="" type="checkbox"/> Antibodies
<input type="checkbox"/> Eukaryotic cell lines
<input checked="" type="checkbox"/> Palaeontology and archaeology
<input type="checkbox"/> Animals and other organisms
<input checked="" type="checkbox"/> Clinical data
<input checked="" type="checkbox"/> Dual use research of concern |
|-----|--|

Methods

- | | |
|-----|---|
| n/a | <input type="checkbox"/> Involved in the study
<input checked="" type="checkbox"/> ChIP-seq
<input type="checkbox"/> Flow cytometry
<input checked="" type="checkbox"/> MRI-based neuroimaging |
|-----|---|

Antibodies

Antibodies used

Anti-chick VEGFA (ABCyclonal, WG-04988), 1:500 dilution.
 Anti-Calnexin (Abcam, ab22595), RRID:AB_2069006, 1:1000 dilution.
 Anti-TSG101(Abcam, ab125011), RRID:AB_10974262, 1:1000 dilution.
 Anti- Chick CSF1R, named Anti- Chick CD115, (Bio RAD,MCA5956GA),clone name:ROS-AV170, 1:100 dilution for flow cytometry.
 Anti chicken CSF1R, named Anti- Chick CD115, ALEX Fluor 647(Bio RAD,MCA5956A647), clone name:ROS-AV170, 1:100 dilution for flow cytometry.
 Anti chicken CSF1R, named Anti- Chick CD115, ALEX Fluor 488(Bio RAD,MCA5956A488), clone name:ROS-AV170, 1:100 dilution for flow cytometry.
 Anti-Integrin α5(CST, Anti-Integrin α5,4705S), 1:1000 dilution.
 Anti-CXCL12 (LSBio, LS-B943), RRID:AB_969159, 1:500 dilution.
 Anti-NDST1 (Santa Cruz biotechnology, sc-374529), RRID:AB_10989196, 1:2000 dilution.
 Anti-CPQ (Sigma-Aldrich, HPA023235), RRID:AB_1855257, 1:500 dilution.
 Anti-GAPDH (Proteintech Group, 60004-1-Ig), RRID: AB_2107436, 1:1000 dilution.
 Anti-KUL01 (Southernbiotech, 8420-09), RRID:AB_2796566, 1:100 dilution for flow cytometry.
 Anti-CCR2 (Thermo, PA5-23037, USA), RRID:AB_11153363, 0.6ug microinjected into Chicken embryo day6.
 Anti-VEGFR2 (Thermo, MA5-15157, USA), RRID:AB_10986085, 1:1000 dilution.
 Anti-Phospho-VEGFR2 (CST, 2474T, USA), 1:1000 dilution.
 Anti-AKT (CST, #9272, USA), 1:1000 dilution.
 Anti-Phospho-AKT (CST, #9271, USA), 1:1000 dilution.
 Goat-Anti-Mouse Ig Human ads-HRP (Southern Biotech), Cat# 1010-05, RRID: AB_2728714, 1:5000 dilution.
 Goat-Anti-Rabbit Ig Human ads-HRP(Southern Biotech), Cat# 4010-05, RRID: AB_2632593 1:5000 dilution.

Validation

Anti-chicken VEGFA was validated by the manufacturer using immunofluorescence staining and we also checking their localization was consistent with literature reports.
 Anti-Calnexin was validated by the manufacturer using ICC-IF, IP and WB. Species: mouse, rat, human. And this antibody has been validated by previous study using WB (Zhao X. et al., Cell Discov, 2019).
 Anti-TSG101 was validated by the manufacturer using Flow Cyt (Intra), ICC-IF, IP and WB. Species: mouse, rat, human. And this antibody has been validated by previous study using WB (Zhao X. et al., Cell Discov, 2019).
 Anti- Chicken CSF1R was validated by the manufacturer using Flow Cyt (Intra), IHC and IF. Species: chicken. We also checking their localization was consistent with literature reports.
 Anti-Integrin α5 was validated by the manufacturer using WB. And this antibody has been validated by previous study using WB (Zhao X. et al., Cell Discov, 2019).
 Anti-CXCL12 was validated by the manufacturer using WB and IHC. Species: Human, Monkey, Mouse, Bat, Dog, Guinea pig, Horse, Chicken, Xenopus. We also checking their localization was consistent with literature reports.
 Anti-NDST1 was validated by the manufacturer using WB. And this antibody has been validated by previous study using WB (Zhao X. et al., Cell Discov, 2019).
 Anti-CPQ was validated by the manufacturer using WB, ICC, IHC, PA. And this antibody has been validated by previous study using WB (Zhao X. et al., Cell Discov, 2019).
 Anti-GAPDH was validated by the manufacturer using WB. Species reactivity: human, mouse, rat, zebrafish, yeast, plant, beagle, carp, chicken, cow, Cynomorium songaricum Rupr, Cyprinus carpio, deer, dog, Eelworm, H. illucens.
 Anti-KUL01 was validated by the manufacturer using Flow Cyt (Intra) and IHC. Species: Chicken. We also checking their localization was consistent with literature reports.
 Anti-CCR2 was validated by the manufacturer using ICC-IF, IHC and Flow Cyt. Species: human, rat. We also checking their localization and function were consistent with literature reports.
 Anti-VEGFR2 was validated by the manufacturer using WB, ICC-IF, IHC and IP. Species: human, mouse, rat. And this antibody has been validated by our recent study using WB.

Anti-phospho-VEGFR2 was validated by the manufacturer using WB. Species: human, mouse. And this antibody has been validated by our recent study using WB.

Anti-AKT was validated by the manufacturer using WB, IP, IF and Flow Cyt. Species: human, mouse, rat, Hamster, Monkey, Chicken, D. melanogaster, Bovine, Dog, Pig. And this antibody has been validated by our recent study using WB.

Anti-phospho-AKT was validated by the manufacturer using WB, IP, IF and Flow Cyt. Species: human, mouse, rat, Hamster, Monkey, D. melanogaster, Bovine, Dog. And this antibody has been validated by our recent study using WB.

The antibody dilution ratio has been specified in methods.

Goat-Anti-Mouse Ig Human ads-HRP were validated by the manufacturer using western blot. Specificity: Reacts with the heavy and light chains of mouse IgG1, IgG2a, IgG2b, IgG2c, IgG3, IgM, and IgA.

Goat-Anti-Rabbit Ig Human ads-HRP were validated by the manufacturer using western blot. Specificity: Reacts with the heavy and light chains of rabbit IgG and IgM.

Eukaryotic cell lines

Policy information about [cell lines and Sex and Gender in Research](#)

Cell line source(s)	HUVECs (human umbilical vein endothelial cells), ScienCell, Cat #8000.
Authentication	The HUVECs were not authenticated.
Mycoplasma contamination	The HUVECs were not tested for mycoplasma contamination.
Commonly misidentified lines (See ICLAC register)	No cell lines used in this study were found in the database of commonly misidentified cell lines that is maintained by ICLAC and NCBI Biosample.

Palaeontology and Archaeology

Specimen provenance	Provide provenance information for specimens and describe permits that were obtained for the work (including the name of the issuing authority, the date of issue, and any identifying information). Permits should encompass collection and, where applicable, export.
Specimen deposition	Indicate where the specimens have been deposited to permit free access by other researchers.
Dating methods	If new dates are provided, describe how they were obtained (e.g. collection, storage, sample pretreatment and measurement), where they were obtained (i.e. lab name), the calibration program and the protocol for quality assurance OR state that no new dates are provided.
<input type="checkbox"/> Tick this box to confirm that the raw and calibrated dates are available in the paper or in Supplementary Information.	
Ethics oversight	Identify the organization(s) that approved or provided guidance on the study protocol, OR state that no ethical approval or guidance was required and explain why not.

Note that full information on the approval of the study protocol must also be provided in the manuscript.

Animals and other research organisms

Policy information about [studies involving animals; ARRIVE guidelines](#) recommended for reporting animal research, and [Sex and Gender in Research](#)

Laboratory animals	Chick embryo are used to conduct TSPAN4 KO and McCherry KI chimera, also CAM angiogenesis assay. All Fertilized SPF eggs (variety: White Leghorn; cleanliness: SPF) were bought from Beijing Boehringer Ingelheim Vital Biotechnology Co., Ltd. All SPF chick embryos used in the study were from embryonic 18h to embryonic day 15. The eggs were incubated in a hatching incubator at 37.5 °C with 60-70% humidity and turned every 5 minutes.
Wild animals	None of the wild animals used.
Reporting on sex	This study did not involve samples collected from sex or gender, since we could not distinguish the gender in SPF hatching eggs and Lack of sex- or gender- based analysis was no relevant to the results.
Field-collected samples	This study did not involve samples collected from field.
Ethics oversight	Use of all chick embryos was according to the guidelines from the Animal Care and Use Committee of Tsinghua University.

Note that full information on the approval of the study protocol must also be provided in the manuscript.

Clinical data

Policy information about [clinical studies](#)

All manuscripts should comply with the ICMJE [guidelines for publication of clinical research](#) and a completed [CONSORT checklist](#) must be included with all submissions.

Clinical trial registration	<i>Provide the trial registration number from ClinicalTrials.gov or an equivalent agency.</i>
Study protocol	<i>Note where the full trial protocol can be accessed OR if not available, explain why.</i>
Data collection	<i>Describe the settings and locales of data collection, noting the time periods of recruitment and data collection.</i>
Outcomes	<i>Describe how you pre-defined primary and secondary outcome measures and how you assessed these measures.</i>

Dual use research of concern

Policy information about [dual use research of concern](#)

Hazards

Could the accidental, deliberate or reckless misuse of agents or technologies generated in the work, or the application of information presented in the manuscript, pose a threat to:

No	Yes
<input type="checkbox"/>	<input type="checkbox"/> Public health
<input type="checkbox"/>	<input type="checkbox"/> National security
<input type="checkbox"/>	<input type="checkbox"/> Crops and/or livestock
<input type="checkbox"/>	<input type="checkbox"/> Ecosystems
<input type="checkbox"/>	<input type="checkbox"/> Any other significant area

Experiments of concern

Does the work involve any of these experiments of concern:

No	Yes
<input type="checkbox"/>	<input type="checkbox"/> Demonstrate how to render a vaccine ineffective
<input type="checkbox"/>	<input type="checkbox"/> Confer resistance to therapeutically useful antibiotics or antiviral agents
<input type="checkbox"/>	<input type="checkbox"/> Enhance the virulence of a pathogen or render a nonpathogen virulent
<input type="checkbox"/>	<input type="checkbox"/> Increase transmissibility of a pathogen
<input type="checkbox"/>	<input type="checkbox"/> Alter the host range of a pathogen
<input type="checkbox"/>	<input type="checkbox"/> Enable evasion of diagnostic/detection modalities
<input type="checkbox"/>	<input type="checkbox"/> Enable the weaponization of a biological agent or toxin
<input type="checkbox"/>	<input type="checkbox"/> Any other potentially harmful combination of experiments and agents

ChIP-seq

Data deposition

Confirm that both raw and final processed data have been deposited in a public database such as [GEO](#).

Confirm that you have deposited or provided access to graph files (e.g. BED files) for the called peaks.

Data access links

May remain private before publication.

For "Initial submission" or "Revised version" documents, provide reviewer access links. For your "Final submission" document, provide a link to the deposited data.

Files in database submission

Provide a list of all files available in the database submission.

Genome browser session (e.g. [UCSC](#))

Provide a link to an anonymized genome browser session for "Initial submission" and "Revised version" documents only, to enable peer review. Write "no longer applicable" for "Final submission" documents.

Methodology

Replicates

Describe the experimental replicates, specifying number, type and replicate agreement.

Sequencing depth

Describe the sequencing depth for each experiment, providing the total number of reads, uniquely mapped reads, length of reads and

Sequencing depth	whether they were paired- or single-end.
Antibodies	Describe the antibodies used for the ChIP-seq experiments; as applicable, provide supplier name, catalog number, clone name, and lot number.
Peak calling parameters	Specify the command line program and parameters used for read mapping and peak calling, including the ChIP, control and index files used.
Data quality	Describe the methods used to ensure data quality in full detail, including how many peaks are at FDR 5% and above 5-fold enrichment.
Software	Describe the software used to collect and analyze the ChIP-seq data. For custom code that has been deposited into a community repository, provide accession details.

Flow Cytometry

Plots

Confirm that:

- The axis labels state the marker and fluorochrome used (e.g. CD4-FITC).
- The axis scales are clearly visible. Include numbers along axes only for bottom left plot of group (a 'group' is an analysis of identical markers).
- All plots are contour plots with outliers or pseudocolor plots.
- A numerical value for number of cells or percentage (with statistics) is provided.

Methodology

Sample preparation	CAM tissue were minced, then digested by collagenase II. All cell mixture were incubated by CSF1R (CD115)-Alex488/ and isolated by Flow cyto.
Instrument	MoFlo Astrios EQ or MoFlo XDP (beckMan)
Software	CytoFLEX S or CytoFlex LX
Cell population abundance	After flowcytometry, cells were devided into two groups, one was CSF1R (CD115) positive, the other was CSF1R (CD115) negative. The purity of the cell samples was identified by IF using CSF1R antibody.
Gating strategy	Gates were applied to density plots to exclude populations (e.g. debris, dead cells) or to positively select populations for further examination. Blank and Negative control samples were prepared to set negative gates and determine the real positive populations.

Tick this box to confirm that a figure exemplifying the gating strategy is provided in the Supplementary Information.

Magnetic resonance imaging

Experimental design

Design type	Indicate task or resting state; event-related or block design.
Design specifications	Specify the number of blocks, trials or experimental units per session and/or subject, and specify the length of each trial or block (if trials are blocked) and interval between trials.
Behavioral performance measures	State number and/or type of variables recorded (e.g. correct button press, response time) and what statistics were used to establish that the subjects were performing the task as expected (e.g. mean, range, and/or standard deviation across subjects).

Acquisition

Imaging type(s)	Specify: functional, structural, diffusion, perfusion.
Field strength	Specify in Tesla
Sequence & imaging parameters	Specify the pulse sequence type (gradient echo, spin echo, etc.), imaging type (EPI, spiral, etc.), field of view, matrix size, slice thickness, orientation and TE/TR/flip angle.
Area of acquisition	State whether a whole brain scan was used OR define the area of acquisition, describing how the region was determined.
Diffusion MRI	<input type="checkbox"/> Used <input type="checkbox"/> Not used

Preprocessing

Preprocessing software	Provide detail on software version and revision number and on specific parameters (model/functions, brain extraction, segmentation, smoothing kernel size, etc.).
Normalization	If data were normalized/standardized, describe the approach(es): specify linear or non-linear and define image types used for transformation OR indicate that data were not normalized and explain rationale for lack of normalization.
Normalization template	Describe the template used for normalization/transformation, specifying subject space or group standardized space (e.g. original Talairach, MNI305, ICBM152) OR indicate that the data were not normalized.
Noise and artifact removal	Describe your procedure(s) for artifact and structured noise removal, specifying motion parameters, tissue signals and physiological signals (heart rate, respiration).
Volume censoring	Define your software and/or method and criteria for volume censoring, and state the extent of such censoring.

Statistical modeling & inference

Model type and settings	Specify type (mass univariate, multivariate, RSA, predictive, etc.) and describe essential details of the model at the first and second levels (e.g. fixed, random or mixed effects; drift or auto-correlation).
Effect(s) tested	Define precise effect in terms of the task or stimulus conditions instead of psychological concepts and indicate whether ANOVA or factorial designs were used.
Specify type of analysis:	<input type="checkbox"/> Whole brain <input type="checkbox"/> ROI-based <input type="checkbox"/> Both
Statistic type for inference (See Eklund et al. 2016)	Specify voxel-wise or cluster-wise and report all relevant parameters for cluster-wise methods.
Correction	Describe the type of correction and how it is obtained for multiple comparisons (e.g. FWE, FDR, permutation or Monte Carlo).

Models & analysis

n/a	Involved in the study
<input type="checkbox"/>	<input type="checkbox"/> Functional and/or effective connectivity
<input type="checkbox"/>	<input type="checkbox"/> Graph analysis
<input type="checkbox"/>	<input type="checkbox"/> Multivariate modeling or predictive analysis
Functional and/or effective connectivity	Report the measures of dependence used and the model details (e.g. Pearson correlation, partial correlation, mutual information).
Graph analysis	Report the dependent variable and connectivity measure, specifying weighted graph or binarized graph, subject- or group-level, and the global and/or node summaries used (e.g. clustering coefficient, efficiency, etc.).
Multivariate modeling and predictive analysis	Specify independent variables, features extraction and dimension reduction, model, training and evaluation metrics.